X-RAY CRYSTALLOGRAPHIC STUDIES OF THE

CYTOCHROME bc_1 COMPLEX

By

BYRON NORTON QUINN

Bachelor of Science
Langston University
Langston, Oklahoma
1997

Master of Science
Oklahoma State University
Stillwater, Oklahoma
2000

Submitted to the Faculty of the
Graduate College of the
Oklahoma State University
in partial fulfillment of
the requirements for
the Degree of
DOCTOR OF PHILOSOPHY
December, 2006

X-RAY CRYSTALLOGRAPHIC STUDIES OF THE

CYTOCHROME bc_1 COMPLEX

Dissertation Approved:

Chang-An Yu

Dissertation Adviser

Linda Yu

Richard Essenberg

Robert Burnap

A. Gordon Emslie

Dean of the Graduate College

ACKNOWLEDGMENTS

My doctoral committee has been an extremely invaluable asset in my ability to complete the structural analysis of the cytochrome bc_1 complex project. My committee was always available to give encouragement and advice at times when the project presented various challenging problems. I would like to thank my advisor Dr. Chang-An Yu for his help in getting me started in x-ray crystallography, molecular modeling and molecular graphics. Moreover, I am extremely thankful to my other committee members: Dr. Linda Yu, Dr. Richard Essenberg, Dr. Eldon Nelson and Dr. Robert Brunap for all of their help and excellent guidance. I would like to thank all of my friends in the lab for their help, support and friendship. I am extremely grateful to have had the opportunity to work with Dr. Di Xia and Dr. Lothar Esser at the National Institute of Health. Dr.Xia and Dr. Lothar provided me with a wealth of knowledge in the area of x-ray crystallography.

Finally, I would like to thank my parents, brothers, sisters, aunts, uncles and cousins for all of their support and help.

TABLE OF CONTENTS

LIST OF TABLES

Table Page

LIST OF FIGURES

Figure Page

CHAPTER I

CHAPTER I

Introduction

Respiratory Chain

Survival of biological cells depends on the biological cell's ability to generate energy necessary for survival. One of the most intriguing organelles inside eukaryotic cells is the mitochondrion, which is responsible for generating most of the energy required by the cell. Mitochondrion is composed of two membranes, an outer membrane that surrounds the entire mitochondrion and an inner membrane which has a convoluted architecture that encapsulates a space called the mitochondrial matrix. The space between the two membranes is called the inter-membrane space. Four transmembrane electron transfer complexes (commonly called Complex I – IV) and a transmembrane adenosine tri-phosphate (ATP) synthase complex (Complex V) are housed in the inner membrane. Complexes I, III and IV all pump protons from the mitochondrial matrix to the intermembrane space allowing for the build up of a proton gradient across the mitochondrial inner membrane (Figure 1). The proton gradient is used by Complex V for the generation of ATP. The ATP molecule consists of an adenine nucleotide plus two other phosphate groups. ATP transfers energy that is stored in the covalent bond between the third and second phosphate to endergonic reactions in the cell. This covalent bond is known as the "high energy" bond because when it is removed by hydrolysis a significant amount of energy is released. Approximately 7.0 kcal per mole of energy is released from the "high energy" bond, although the exact amount of released energy will depend on the conditions of bond breakage.

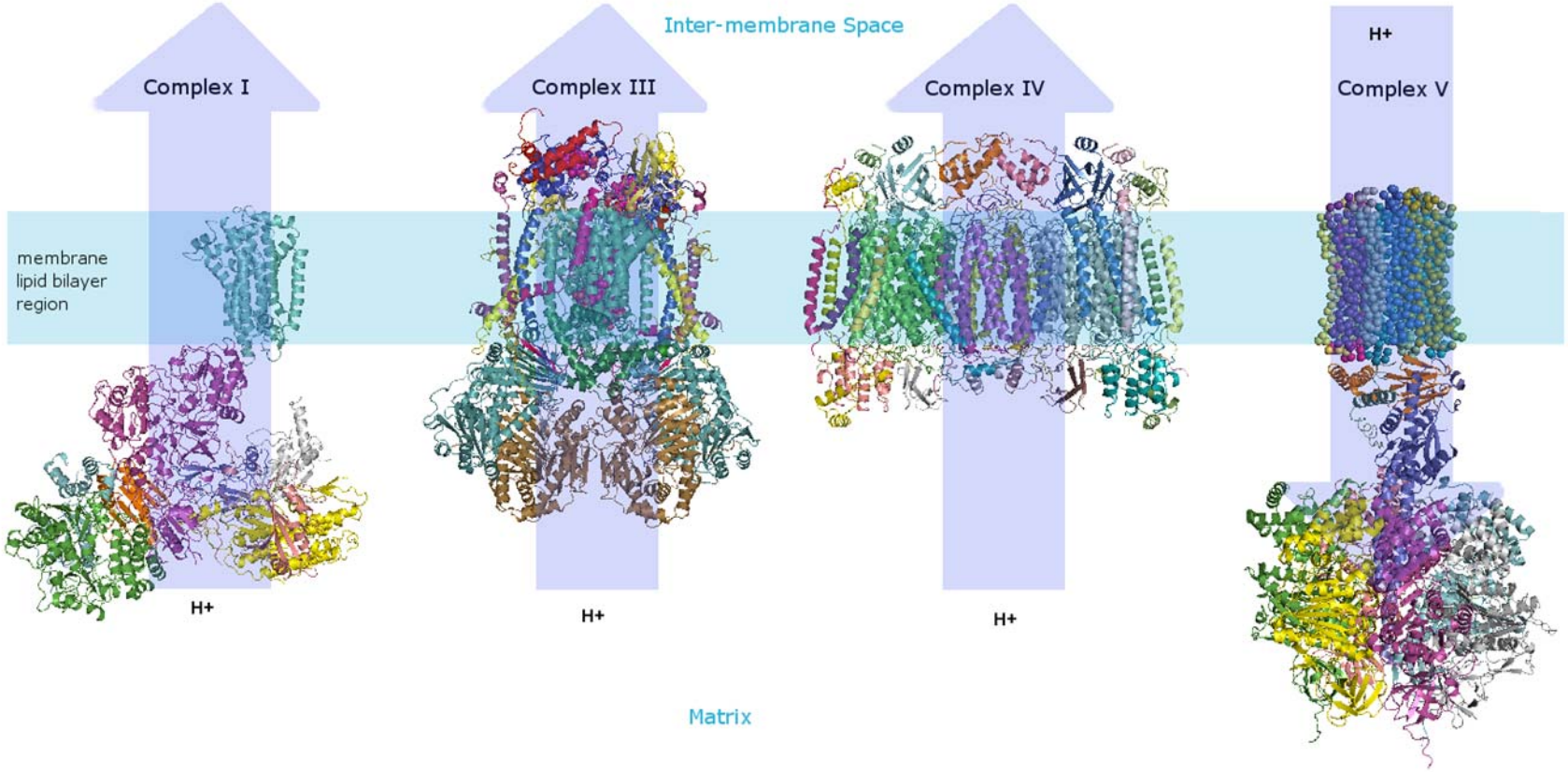

Figure 1. Electron transfer chain. Complex I membrane region is modeled in.

Navigation of electrons through the respiratory chain begins with nicotinamide adenine dinucleotide (NADH) dehydrogenase (Complex I). Complex I is the largest of the electron transport proteins, with 43 subunits and a mass of approximately 900kD. The overall shape of Complex I is similar to the letter "L" with the vertical part of the "L" in the membrane (the stalk) and the lower horizontal part of the "L" (the soluble globular arm) in the matrix, with the exception that the lower horizontal part of Complex I is much larger than the vertical stalk part. Recently the crystal structure of the soluble globular arm of Complex I was solved at 3.3 Å resolution from *Thermus thermophilus*, which contains eight subunits along with all the redox centers of the enzyme, protein data bank (pdb) code (2fug) (1). Complex I allows a pathway for electrons to transfer from the NADH-binding site in the arm to the quinone-binding site in the stalk, resulting in the generation of a quinol molecule from the pool of quinone in the intermembrane space. In the process of Complex I generating a molecule of quinol four protons from the mitochondrial matrix are pumped to the intermembrane space. Several prosthetic groups in Complex I participate in electron transfer allowing for the electron to travel from the NADH binding site to the quinone binding site.

Succinate dehydrogenase (Complex II) is a membrane protein that does not pump protons but it does contribute to the ubiquinol pool. Complex II catalyzes the oxidation of succinate to generate a molecule of ubiquinol. The structure of Complex II has been solved from *Escherichia coli* at a resolution of 3.1 Å (pdb code 2acz) and chicken heart at a resolution of 2.0 Å (2,3) .

Ubiquinol is utilized by ubiquinol cytochrome *c* oxidoreductase (Complex III) or (bc_1 complex) to transfer electrons to the soluble cytochrome *c* in the intermembrane

space along with the translocation of protons from the mitochondrial matrix to the mitochondrial intermembrane space. The functioning of the bc_1 complex is commonly described by the proton motive Q cycle, which is a hypothesis used to describe the navigation of electrons from the electron donor ubiquinol to the electron acceptor cytochrome *c*.

Cytochrome *c* oxidase (Complex IV) is the final enzyme to interact with electrons originating from the oxidation of metabolic fuels. Complex IV is a dimeric transmembrane electron transfer protein consisting of 13 subunits per monomer in the mammalian complex. The crystal structure of Complex IV has been solved at 2.3Å resolution (pdb code 2occ). Complex IV functions by oxidizing the soluble cytochrome *c* and reducing molecular oxygen to water. Complex IV also pumps 4 additional protons from the matrix to the intermembrane space, which would correlate to two protons for every pair of electrons from cytochrome *c*.

Complex V utilizes the proton gradient generated by Complexes I, III and IV to phosphorylate adenosine diphosphate (ADP). Complex V consists of two parts F_1 (the soluble part which resides in the matrix) and F_o (the hydrophobic part which resides in the mitochondrial innermembrane (Figure 1). The F_o part lets the flow of protons back into the matrix and the F_1 part synthesizes the adenosine triphosphate (ATP) from ADP.

The study of the respiratory chain reveals several remarkable aspects of the metabolic process; in particular the way electron transfer complexes couples the transfer of electrons to the translocation of protons. Crystallography has played an important role in deciphering the complex attributes of the electron transfer proteins.

Cytochrome bc_1 Complex

The bovine mitochondrial bc_1 complex is a dimeric transmembrane protein that consists of 11 subunits with a dimeric molecular weight of about 500 kDa (Figure 2) (Table I) (3). The largest subunits in the mitochondrial bc_1 complex as seen in table I are core 1 and core 2. Core1 and core2 have sequence homology to zinc proteases, and function in the cleavage and retention of the iron sulfur protein subunit (ISP) presequence, in which the ISP presequence becomes subunit 9 in the bc_1 complex (4-6).

Three subunits out of the eleven total subunits are essential for electron transfer in Complex III (Figure 4). The three essential subunits are cytochrome *b* (cyt. *b*) which contains low and high potential *b*-type hemes (b_L and b_H), cytochrome c_1 (cyt. c_1) which contains a c-type heme, and ISP which contains a 2Fe-2S cluster (FeS). Distances between the hemes and the FeS are shown in figure 5. The bacterial bc_1 complex in *Rhodobacter sphaeroides* contains homologues of the three essential subunits from bovine and supernumerary fourth subunit termed subunit 4. *Rodobacter capsulatus* bacterial bc_1 complex only contains 3 subunits which are the homologues of the three essential subunits in bovine. The x-ray crystal structure for the *Rodobacter capsulatus* bc_1 complex has been solved at 3.5 Å resolution and reveals the identity of structurally conserved regions in the bc_1 complex (7). Site-directed mutagenesis studies in bacterial bc_1 complexes have significantly advanced the study of deciphering the important role conserved residues play in the bc_1 complex.

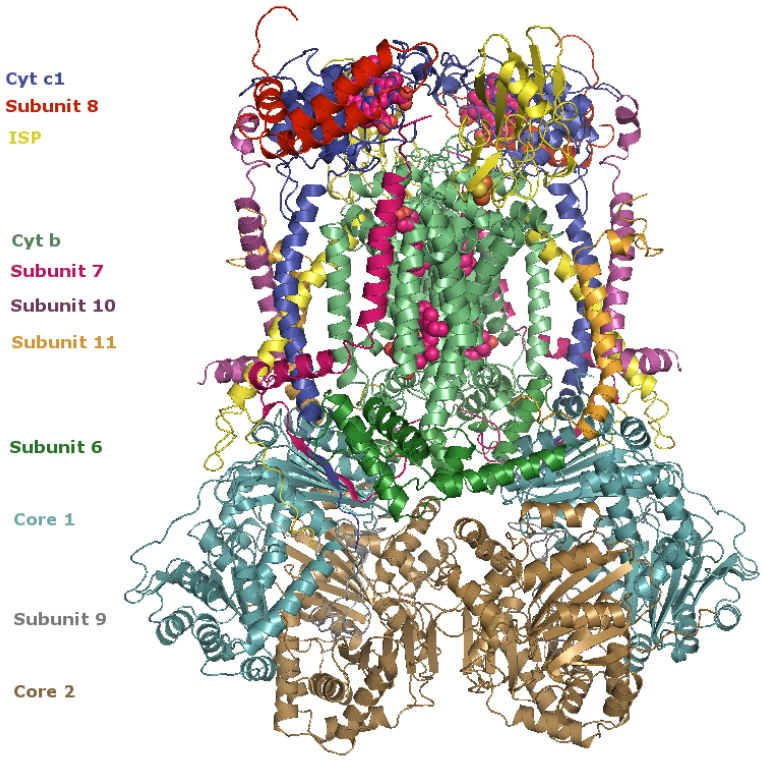

A

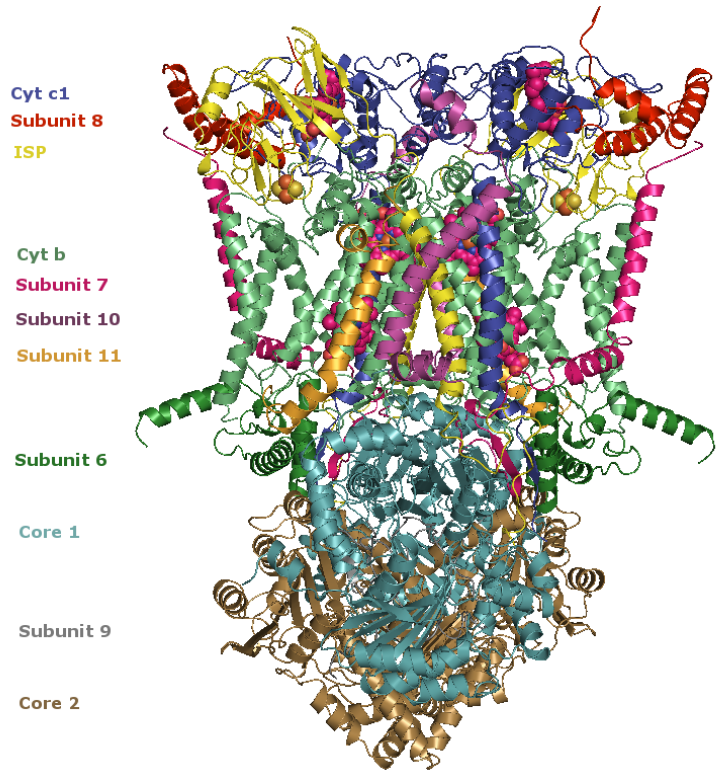

B

Figure 2. Bovine bc_1 Complex. (B) is a ninety degree rotation of (A).

Table I. Subunits of the bovine bc_1 complex

Subunit	Name	aa[a]	ID[b]
1	Core 1	446	P31800
2	Core 2	439	P23004
3	Cyt. *b*	379	P00157
4	Cyt c_1	241	223266
5	ISP	196	P13272
6	QPK	110	P00129
7	QPC	81	P13271
8	Hinge	78	P00126
9	Subunit 9	57	P13272
10	Subunit 10	62	P00130
11	Subunit 11	56	P07552

[a] Number of amino acid residues
[b] Genebank accession number

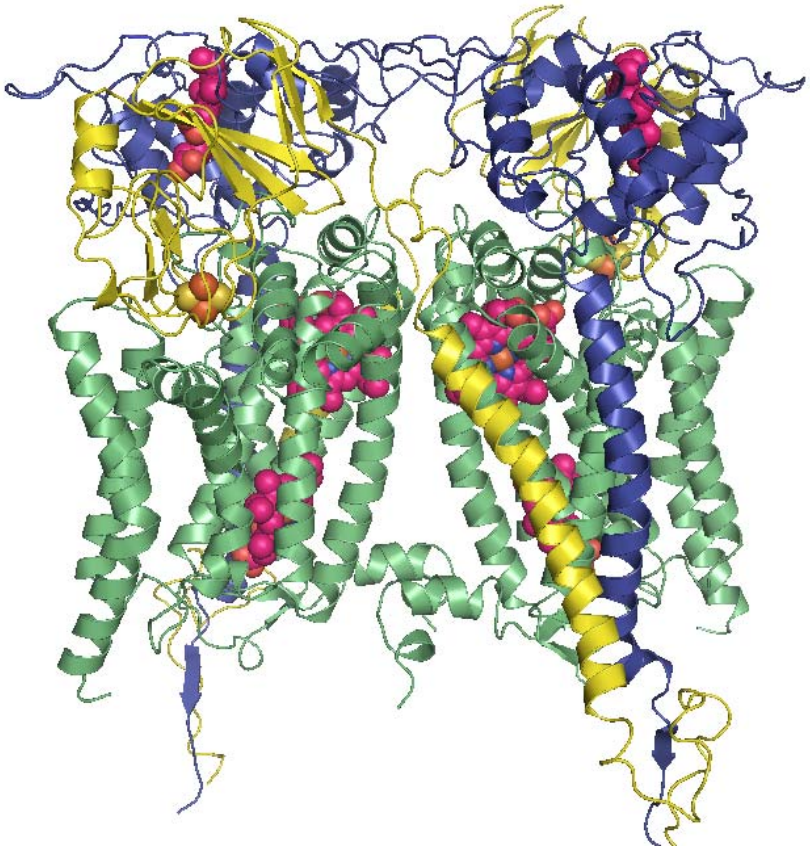

Figure 3. Dimer of the three essential subunits in the bc_1 complex. Where cyt *b* is green and represents the membrane region, ISP is yellow, and cyt c_1 is blue.

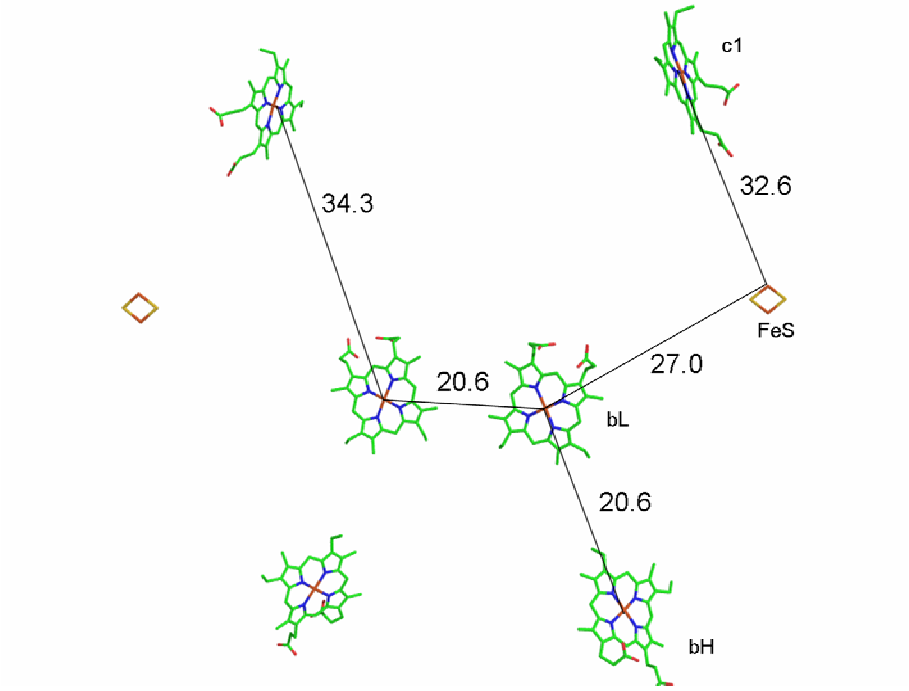

Figure 4. Distances between iron atoms in angstroms.

The first three-dimensional atomic level resolution crystal structure of cytochrome bc_1 complex from bovine heart mitochondria was solved at 2.9 Å resolution where majority of the bc_1 complex was modeled in including core 1, core 2, cyt. *b*, subunit 6, subunit 7, a carboxyl-terminal fragment of cyt. c_1, and an amino-terminal fragment of ISP (8). Afterwards, more complete bc_1 complex structures were reported (9-11).

The subunit which houses the bc_1 complex substrates and various inhibitors is cyt. *b* which has eight alpha helices labeled A-H, and resides mainly in the membrane (Figure 6). Helices B and D contain the histidine residues which are responsible for holding cyt. b_L heme and cyt. b_H heme in place. A surface rendering of the cytochrome *b* subunit reveals 4 major cavities as depicted in figure 6. The ISP head domain docking cavity exterior is defined by cyt *b* residues Trp141, Thr144, Ser151, Ser169, Leu262, Thr264, Pro266, Pro285, Lys287, Val343 which is where the ISP head domain that contains the FeS docks. The exterior of the Q_o site cavity is defined by cyt. *b* residues Ile146, Leu149, Phe274, Val291, Leu294. The Q_m site cavity exterior is defined by residues Trp30, Ile92, Met96, Trp272, Trp326, Val329, Leu333, Thr336 and the Q_i site cavity exterior consists of residues Phe18, Ile39, Ile42, Met194. The Q_o and Q_i sites are binding sites for the substrates ubiquinol and ubiquinone respectively. The inhibitors for the bc_1 complex have been categorized as P or N to denote which binding site the inhibitors bind in, P for the Q_o site and N for the Q_i site (Figure 7) (12,13). The Q_o site inhibitors have been further classified as P_f for the ability to fix the ISP head domain and P_m if the inhibitor keeps the ISP head domain in the mobile state (12).

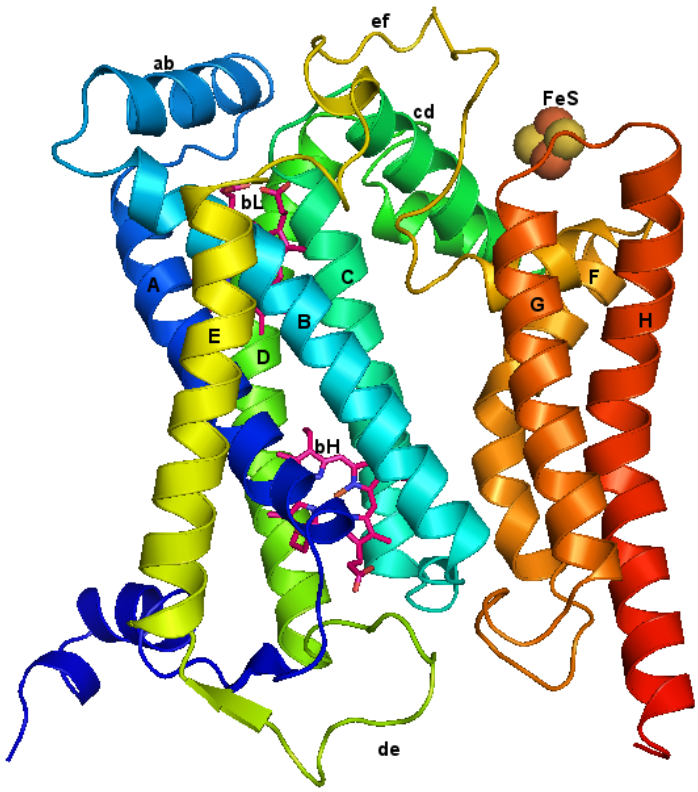

Figure 5. Cytochrome *b* labeled helixes.

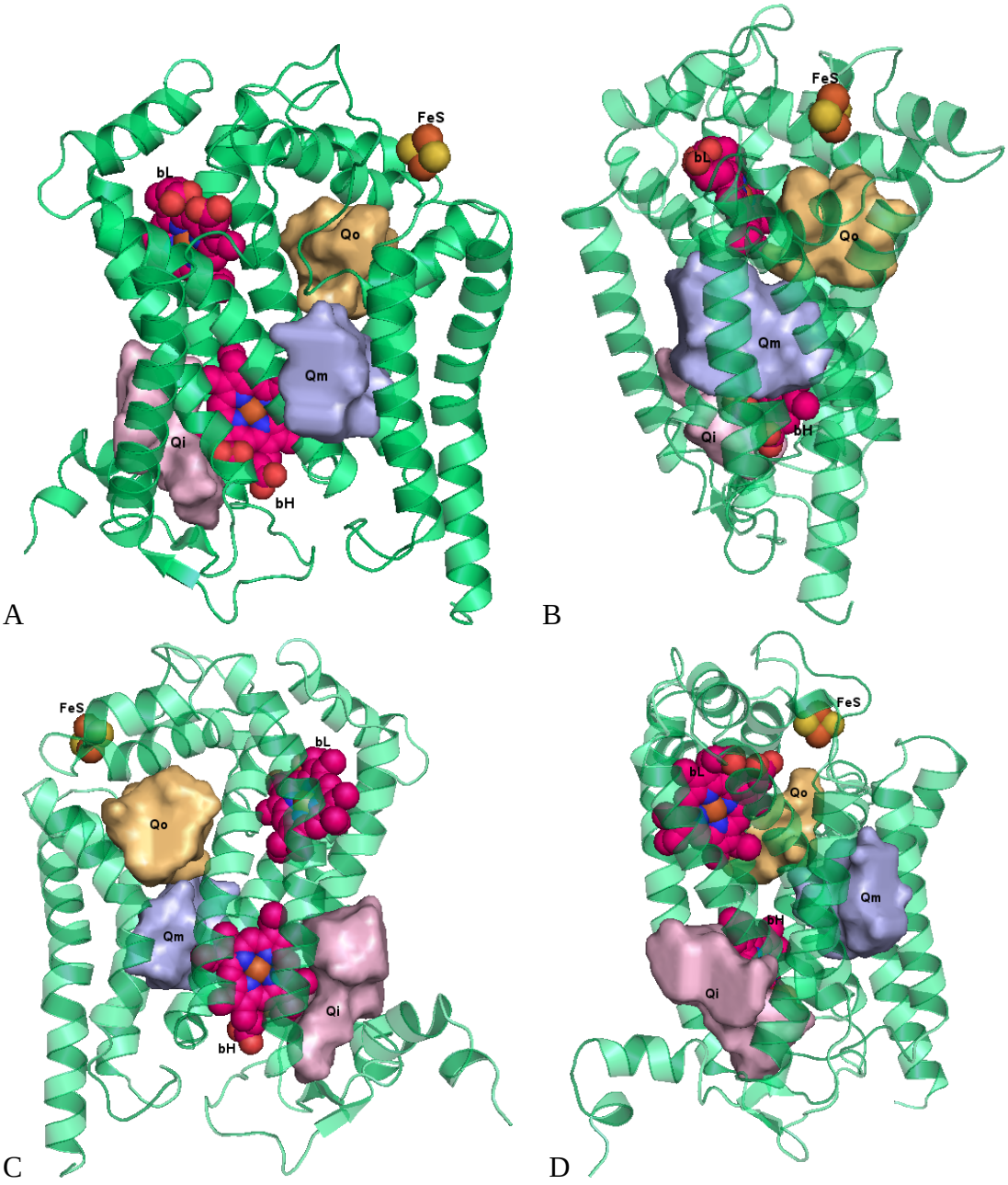

Figure 6. Major cavities in cytochrome *b*. (B) is a 90 rotation of (A), (C) is a 90 degree rotation of (B), and (D) is a 90 rotation of (C). ISP head domain docking cavity is at the FeS position.

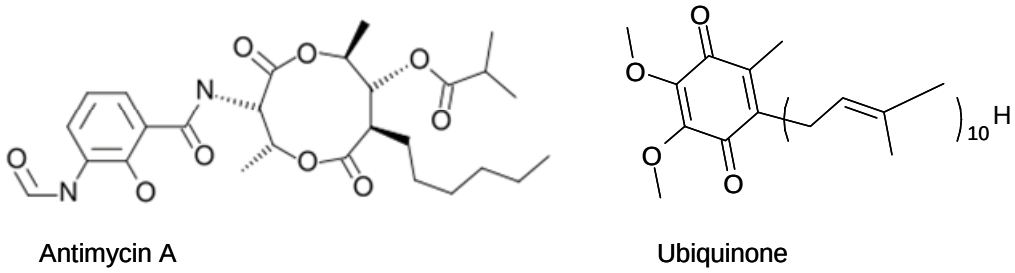

A. Q_i site inhibitor antimycin A and substrate ubiquinone.

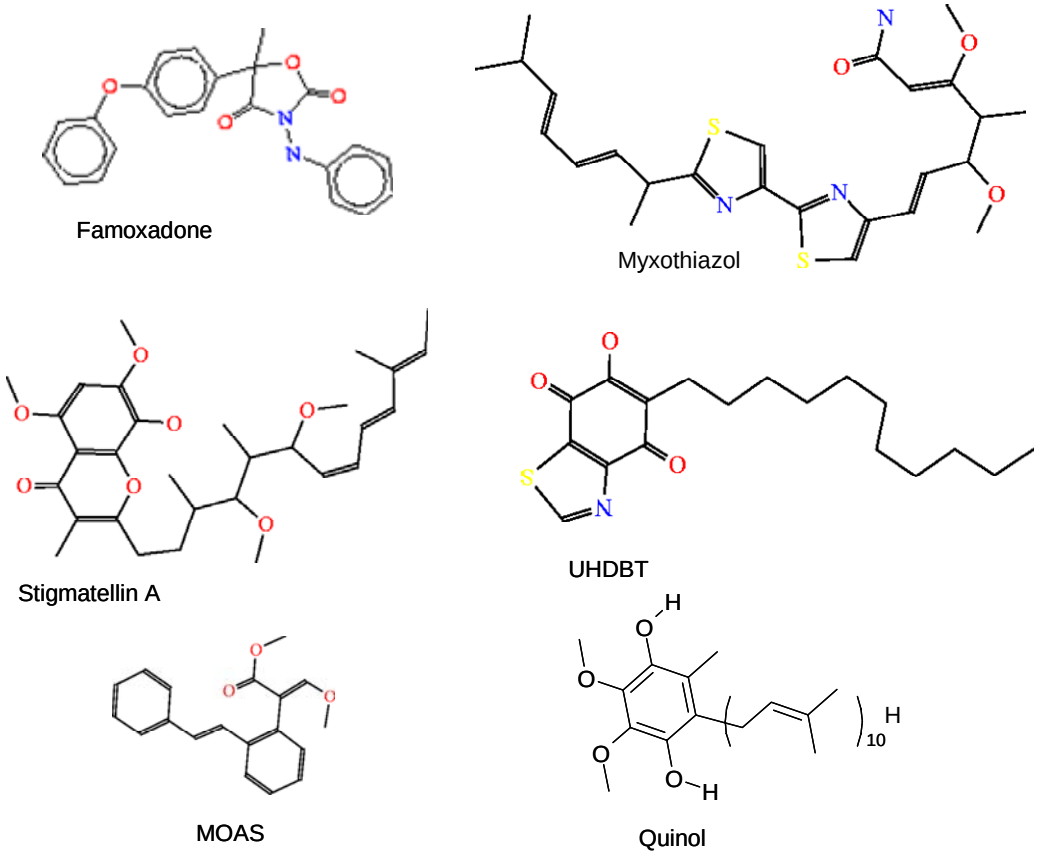

B. Q_o site inhibitors, and substrate quinol.

Figure 7. *bc*$_1$ complex inhibitors and substrates.

The Q_o Site

The Q_o substrate binding site of the native bc_1 has a shape similar to that of a funnel (14). The outside of the binding site has a relatively wide opening and the cross sectional area becomes narrower moving inward. The Q_o binding site is highly hydrophobic and surrounded by aromatic residues in addition to a number of aliphatic residues. The top of the Q_o binding site is capped off with His161, which is part of the 2Fe-2S cluster in the ISP subunit, when the ISP head domain is docked onto the cytochrome *b* subunit. The Q_o binding site has a considerable amount of conserved residues that may interact with the substrate in a manor similar to that of the inhibitors during the various functional stages of enzymatic activity.

MOAS in the Q_o binding site

MOAS, 3-methoxy-2-(2-styryl-phenyl)-acrylic acid methyl ester, consists of a methoxy methyl acrylate group (toxophore) and a stilbene moiety (Figure 7). MOAS is derived from strobilurin and is a synthetic anti-fungal agent. One hydrogen bond is formed between the backbone amide group of Glu271 and the oxygen atom O3 in MOAS. The binding environment for MOAS consists of several aromatic residues, Phe274, Phe128, Tyr273, and Tyr131. A parallel displaced pi-stacking interaction is formed between the aromatic ring of Phe274 and the styryl moiety of MOAS. The binding of MOAS in the Q_o binding site is shown in the LIGPLOT representation (Figure 8)(15).

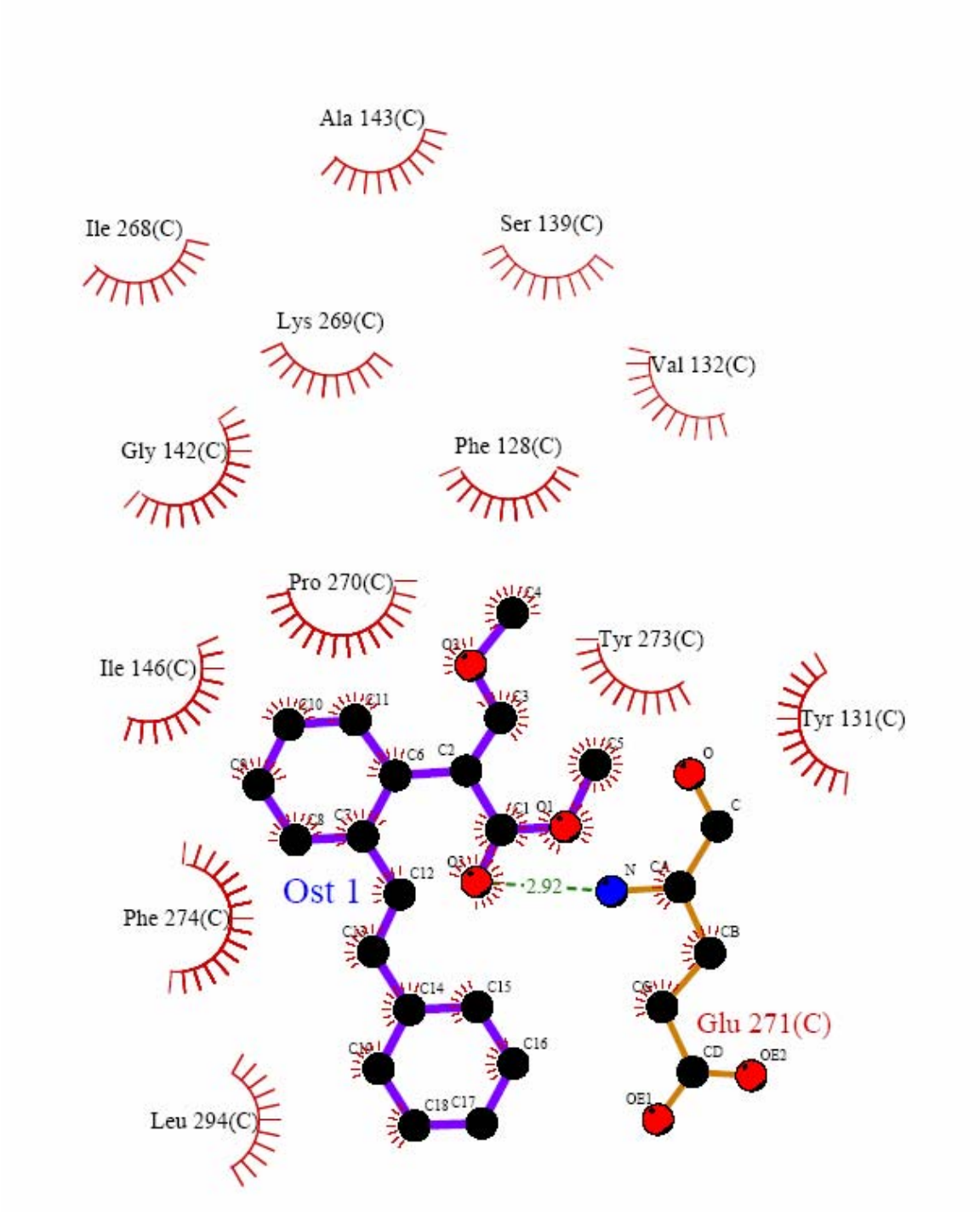

Figure 8. MOAS binding in the Q_o site.

Interactions shown in the LIGPLOT representation are those mediated by hydrogen bonds and by hydrophobic contacts. Hydrogen bonds are indicated by dashed lines between the atoms involved, while hydrophobic contacts are represented by an arc with spokes radiating towards the ligand atoms they contact (15). The contacted atoms are shown with spokes radiating back. The LIGPLOT representation is a two-dimensional representation of how the ligand is binding in the binding site of the enzyme. LIGPLOT representation of the binding site allows for a quick analysis of important contacts between the ligand and residues in the binding site. In the LIGPLOT representation all residues interacting with the ligand are shown. Three-dimensional figures will typically have residues that make up the binding site removed to allow for the viewing of the substrate with hydrogen bonding residues. The three-dimensional viewing is best achieved with molecular graphics software.

Myxothiazol in the Q_o site.

Myxothiazol is an anti-fungal inhibitor that is produced by myxobacterium *Myxococcus fulvus*. Myxothiazol has an active methoxyacrylamide group and a dithiazole moiety. An amide functional group is one of the characteristics that separate myxothiazol from other MOA type inhibitors. Phe274 may play a role in aromatic-aromatic interactions with the diathiazol moiety to stabilize myxothiazol in the binding site. Two hydrogen bonds are formed between myxothiazol and residues in the Q_o site. A hydrogen bond is formed between the hydroxyl group of Tyr273 and the amide nitrogen atom N1 of myxothiazol. The second hydrogen bond is formed between the backbone amide of Glu271 and the amide oxygen atom O1 of myxothiazol. The binding of myxothiazol in the Q_o binding site is shown in figure 9.

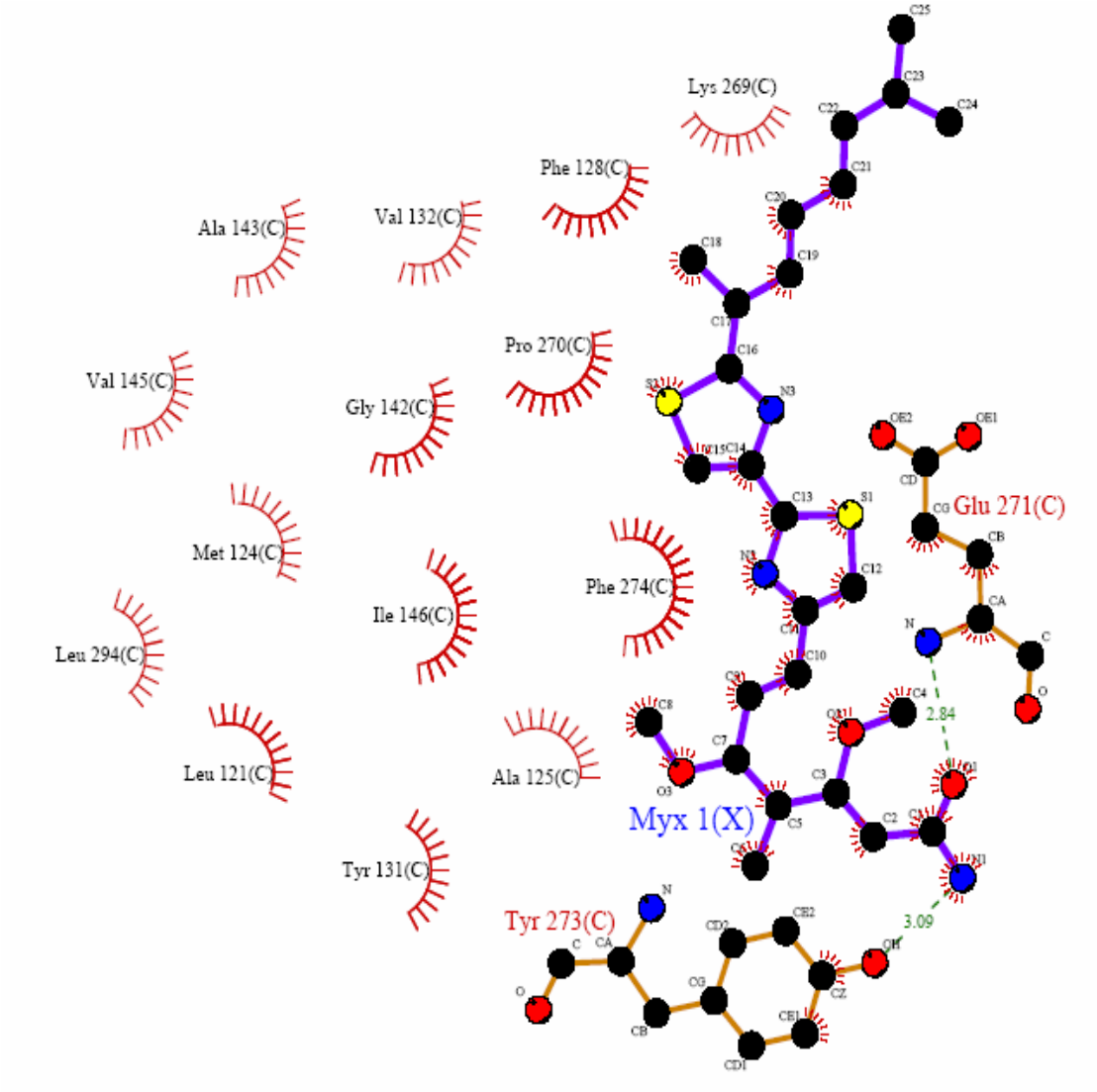

Figure 9. Myxothiazol binding in the Q_o site.

Famoxadone in the Q_o binding site

Famoxadone, 5-methyl-5-(4-phenoxy-phenyl)-3- phenylamino-2,4 oxazolidinedione, is a Q_o site bc_1 complex inhibitor(Figure 7). One hydrogen bond is found between famoxadone oxygen atom O6 of the oxazolidine-2,4- dione ring and the amide group of Glu271 with a distance of 2.57 Å. A hydrogen bond is also possible between the secondary amine N2 of famoxadone and a water molecule. The famoxadone, hydrogen bonding, water molecule is also in hydrogen bonding distance to Lys269 and Tyr131 (14). Famoxadone in the Q_o binding site is surrounded by several aromatic residues, which help to establish a network of aromatic-aromatic interactions between famoxadone and the binding site. The aromatic residues in the Q_o binding site may play a role in stabilizing the substrate in the binding site and also play a role in facilitating electron transfer. The binding of famoxadone in the Q_o binding site can be seen in figure 10.

UHDBT in the Q_o binding site

UHDBT is a benzoquinone derivative and of all the Q_o site inhibitors considered, UHDBT is the closest structural analog to quinol (Figure 7). Wedged between Pro270 and Val145, is the hydroxyl dioxobenzothiazole moiety of UHDBT. One hydrogen bond is formed between Tyr131 and the O4 hydroxyl group of UHDBT (Figure 11). It is possible that when the extrinsic head domain of ISP is positioned in the b-position the protonated His161 of ISP may form a hydrogen bond with the carbonyl oxygen O7 of UHDBT. A deprotonated His161may form a hydrogen bond with the hydroxyl O6 of UHDBT.

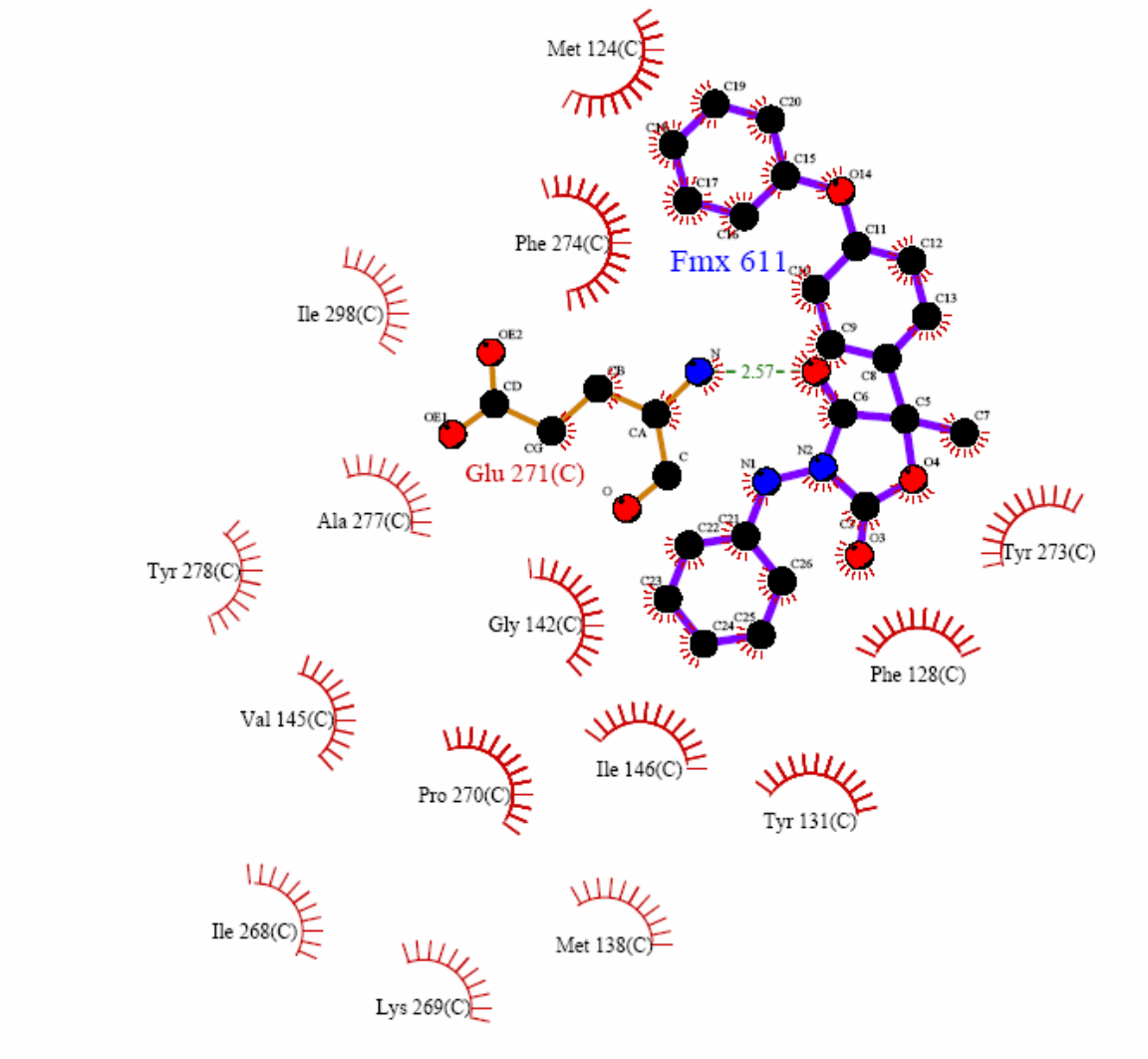

Figure 10. Famoxadone binding in the Q_o site.

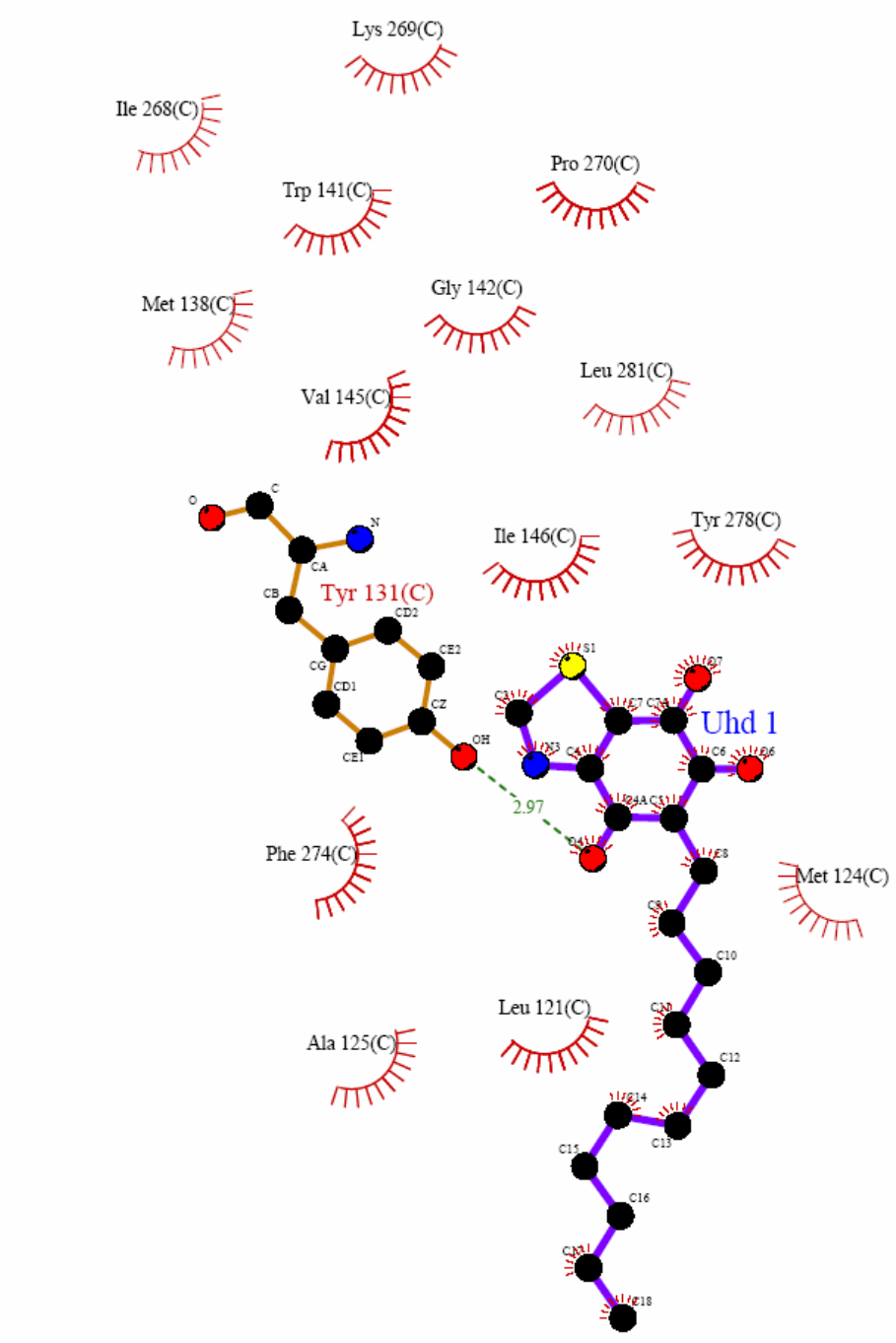

Figure 11. UHDBT binding in the Q_o site.

Stigmatellin in the Q_o binding site

Stigmatellin is a natural anti-fungal inhibitor produced by myxobacteria *S. aurantiaca* (Figure 7). The binding of stigmatellin in the Q_o binding site relies on the head domain of ISP being docked in the b-postition (16). The crystal structure of stigmatellin has been solved in several pdb files. In the pdb file 1sqx (2.6 Å resolution) the protonated atom NE2 of His161 of ISP forms two hydrogen bonds with both the methoxy oxygen (O5) and carbonyl group (O4) of the inhibitor with distances of 3.5 Å and 3.4 Å, respectively (12). A hydrogen bond (2.6 Å) is formed between the hydroxyl group O8 of stigmatellin and atom OE2 of Glu271 whose side-chain undergoes a rotation around chi1 of, ~160^o from its native position(12) (Figure 12). In a higher resolution (2.1 Å) crystallographic structure of the bc_1 complex with stigmatellin (pdb code 2a06) His161 of ISP has moved closer to the stigmatellin molecule (Figure 13). The hydrogen bonding distance between the His161 and stigmatellin is now 2.68 Å. This difference may be the result of the difference in the resolution of the crystal structures. If this were the case then it would be expected that the hydrogen bonding distance between Glu271 and stigmatellin would be off also. Both crystal structures show about 2.6 Å for this distance. Therefore, another possibility may be that this difference is representative of possible transition states in the reaction pathway. The bc_1 complex has the enormous job of coupling electron transfer with proton pumping, therefore the entrance and exit of the substrate in the active site may require several different geometries of the active site as the reaction proceeds from beginning to completion. Table II shows the correlation of contact residues in the Q_o binding site relative to the inhibitors.

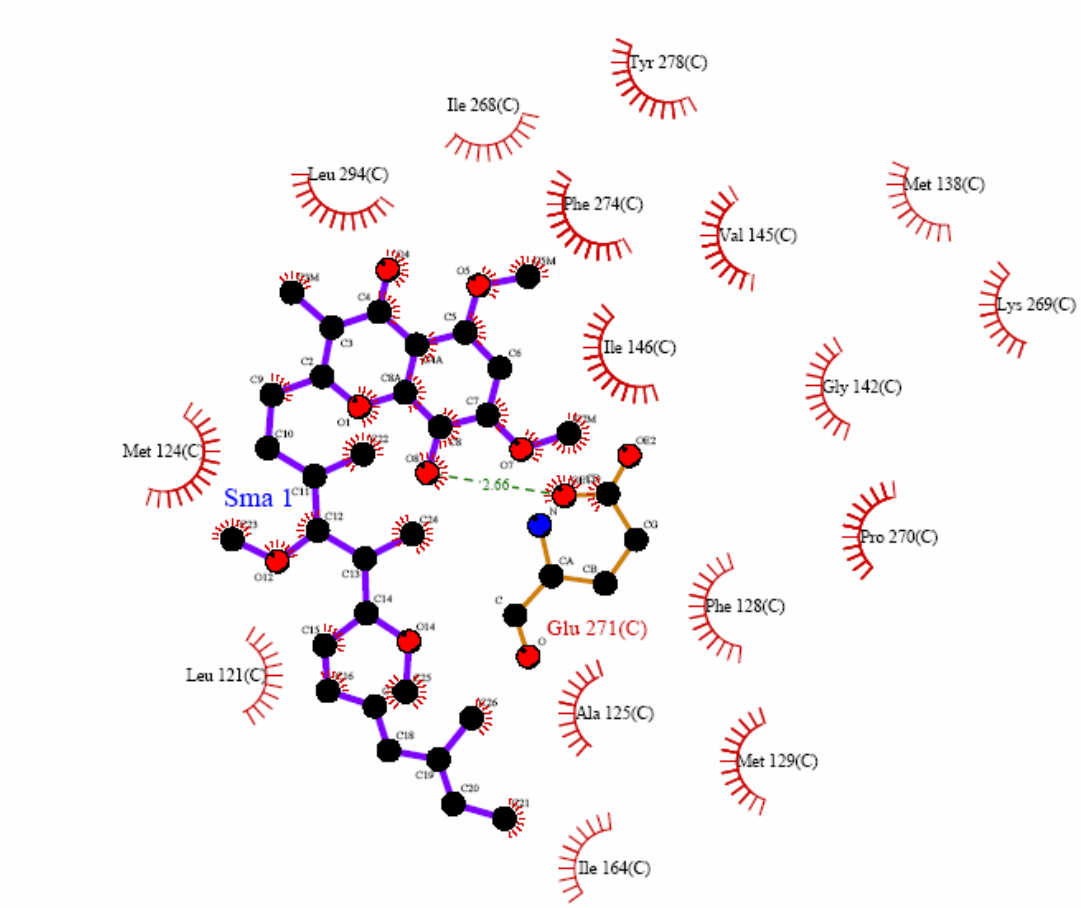

Figure 12. Stigmatellin in the Q_o binding site (pdb code 1sqx).

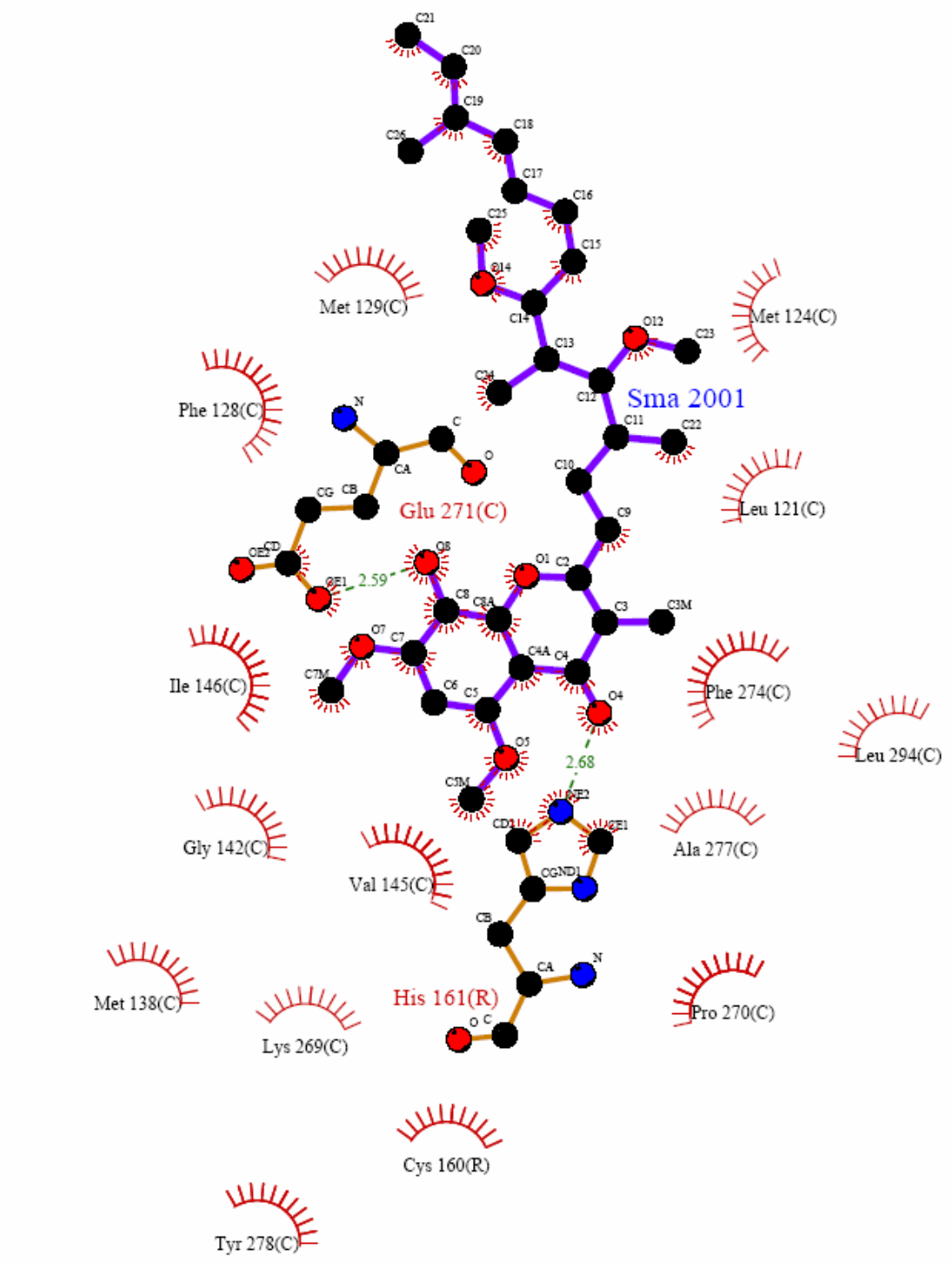

Figure 13. Stigmatellin in the Q_o binding site (pdb code 2a06).

Table II. Q_o Binding Site Residues with Inhibitors

	MOAS	Myzo[a]	Famox[b]	UHDBT	Stig[c]
LEU 121	N	I	N	I	I
MET124	N	I	I	I	I
ALA125	N	I	N	I	I
PHE 128	I	I	I	N	I
MET129	N	N	N	N	I
TYR 131	I	I	I	H	N
VAL 132	I	I	N	N	N
MET 138	N	N	I	I	I
SER 139	I	N	N	N	N
TRP 141	N	N	N	I	N
GLY 142	I	I	I	I	I
ALA 143	I	I	N	N	N
VAL 145	N	I	I	I	I
ILE 146	I	I	N	I	I
ILE 264	N	N	N	N	I
ILE 268	I	N	I	I	I
LYS 269	I	I	I	I	I
PRO 270	I	I	I	I	I
GLU 271	H	H	H	N	H
TYR 273	I	H	I	N	N
PHE 274	I	I	I	I	I
ALA 277	N	N	I	I	N
TYR 278	N	N	I	N	I
LEU 281	N	N	N	I	N
LEU 294	N	I	N	N	I
ILE 298	N	N	I	N	N

[a] Abbreviation for myxothiazol
[b] Abbreviation for famoxadone
[c] Abbreviation for Stigmatellin
The letter I represents a residue that is close enough to "interact" with the inhibitor as revealed in the LIGPLOT representation. N means that "no" interaction was detected in the LIGPLOT representation. And H represents "hydrogen bonding" as detected in the LIGPLOT representation.

The Q_i site

The Q_i binding site is positioned at the matrix side of the membrane. The opening of the Q_i binding site is inward-facing the opposing monomer. Shuttling of the substrate may be facilitated by the geometric locations of the Q_i binding site in one monomer with the Q_o site in the opposing monomer. The overall shape of the Q_i binding site is somewhat like that of a funnel. The outside of the cavity is wide and as you enter into the cavity heading toward the back, the width of the cavity decreases. Residues from helix A, D, and E make up the Q_i binding site along with part of the propionate side chain of the high-potential heme b_H.

Antimycin A in the Q_i binding site

Antimycin A is made up of a nine-member puckered dilactone ring in the middle, a 3-formylamino salicylic acid (3-FASA) group that is connected to the dilactone ring and a hydrophobic tail on the other side of the dilactone ring. There are two crystal structures with slightly different configurations for antimycin A in the Q_i binding site as revealed in pdb codes 1ntk (2.6 Å) and 1ppj (2.1 Å) (Figure 14 and 15). The main difference appears to be a rotation of the nine-membered puckered dialactone ring. This difference may be the result of many different variables. Crystallization conditions between the two data sets are different and may play a role in the rotation of the nine-membered dilactone ring. The overall shape of the two are relatively the same where the 3-formylamino salicylic acid group is positioned deep in side the back of the Q_i binding site, and the nine-membered dialactone ring is positioned more towards the outside of the binding site.

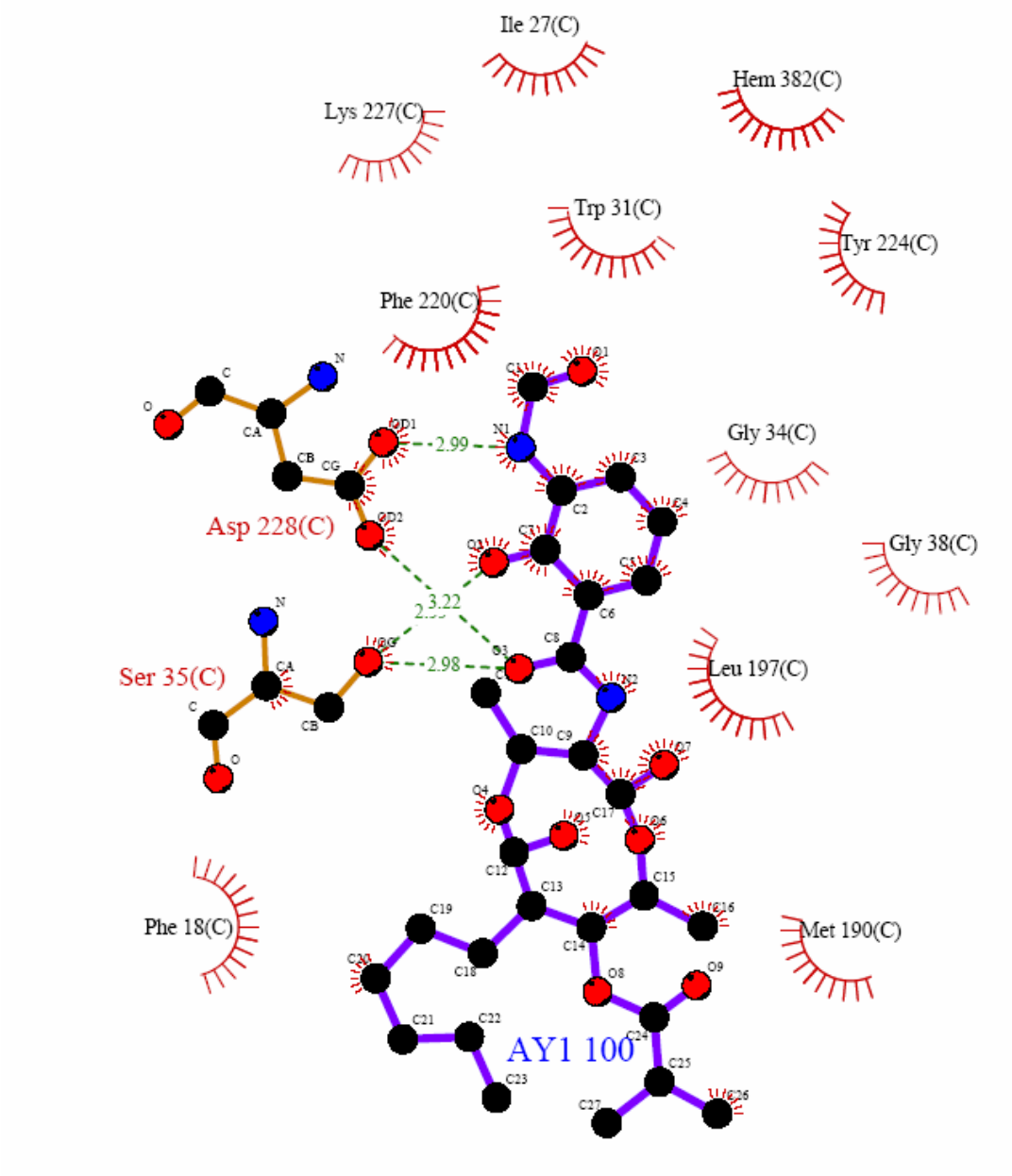

Figure 14. Antimycin binding in the Q_i site (pdb code 1ntk).

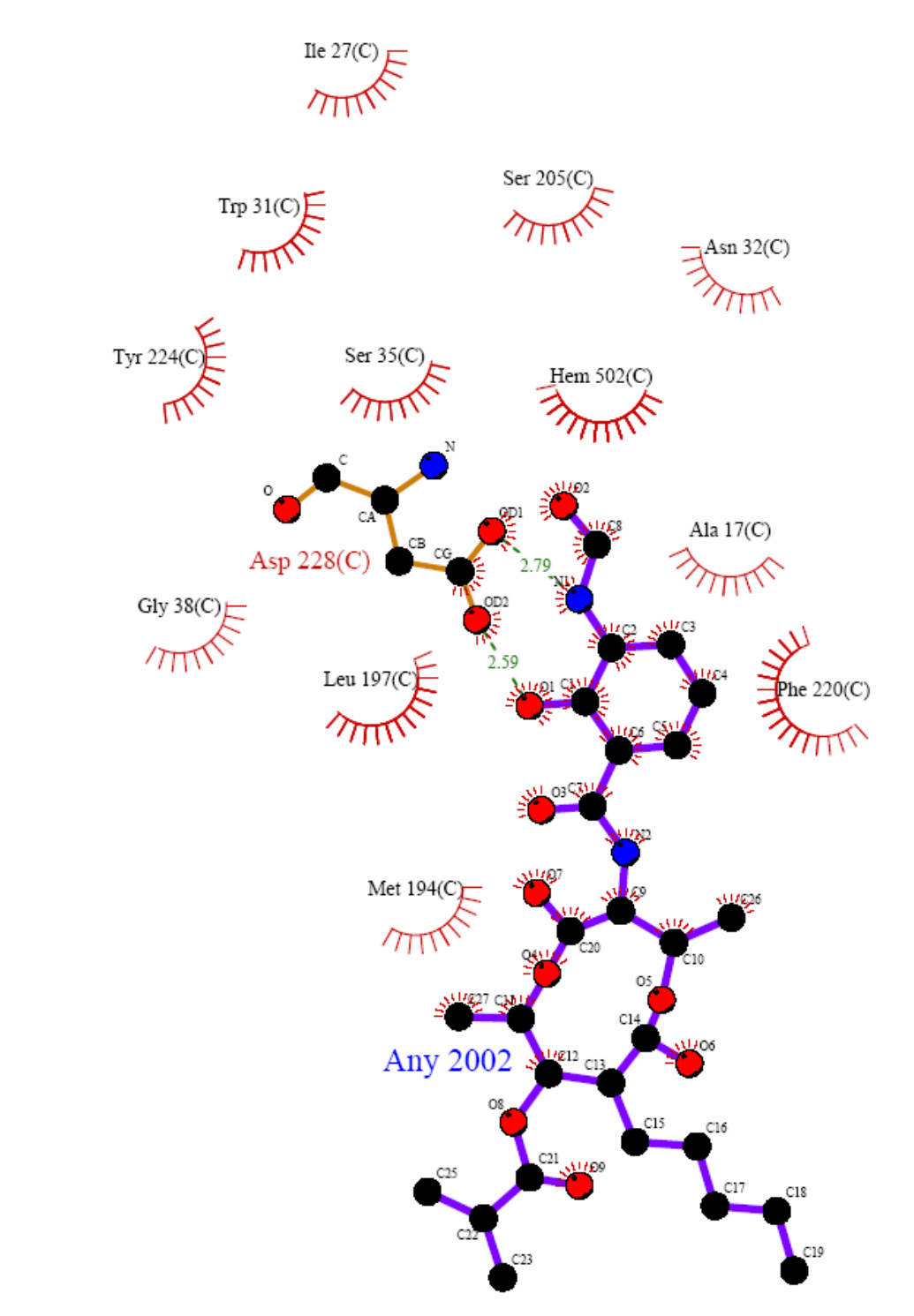

Figure 15. Antimycin binding in the Q_i site (pdb code 1ppj).

Ubiquinone binding in the Q_i site

The crystal structure of ubiquinone co-crystallized with the bc_1 complex is available in pdb files 1sqx (2.6 Å) and 2a06 (2.1 Å) as shown in LIGPLOT representation figures 16 and 17 respectively. Both pdb codes 1sqx and 2a06 have ubiquinone modeled in the Q_i site where the first two isoprenoid units are attached. The head group of the ubiquinone is inserted all the way into the back of the Q_i binding site cavity. Geometrically, the ubiquinone head group is oriented with the methyl group towards His201. Atom NE2 of His201 is able to from a hydrogen bond with the carbonyl oxygen atom next to the methyl group of ubiquinone. Phe220 is oriented such that aromatic-aromatic interactions are possible with ubiquinone in the Q_i binding site. The crystal structures reveal water molecules in the Q_i binding site that may play a role in proton transfer.

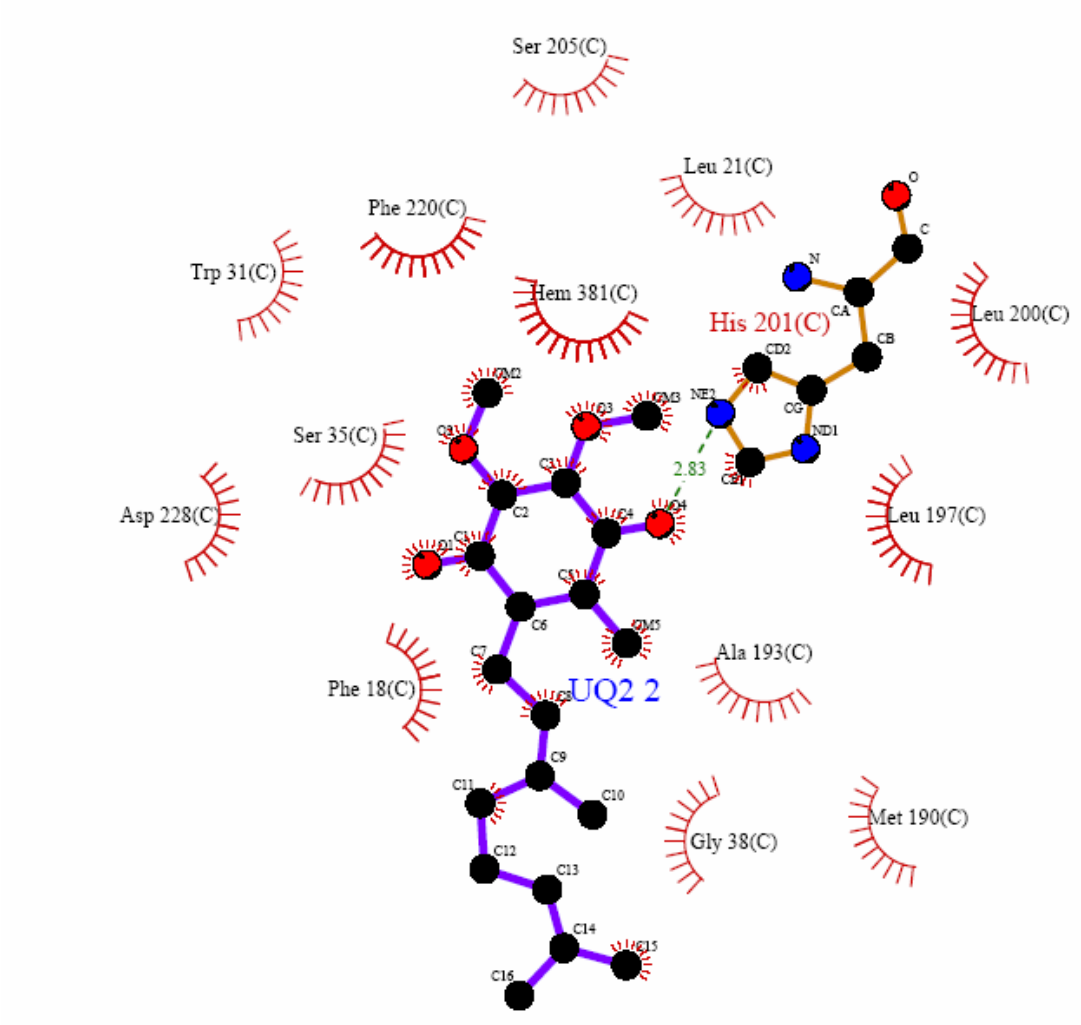

Figure 16. Ubiquinone binding in the Q_i site (pdb code 1sqx)

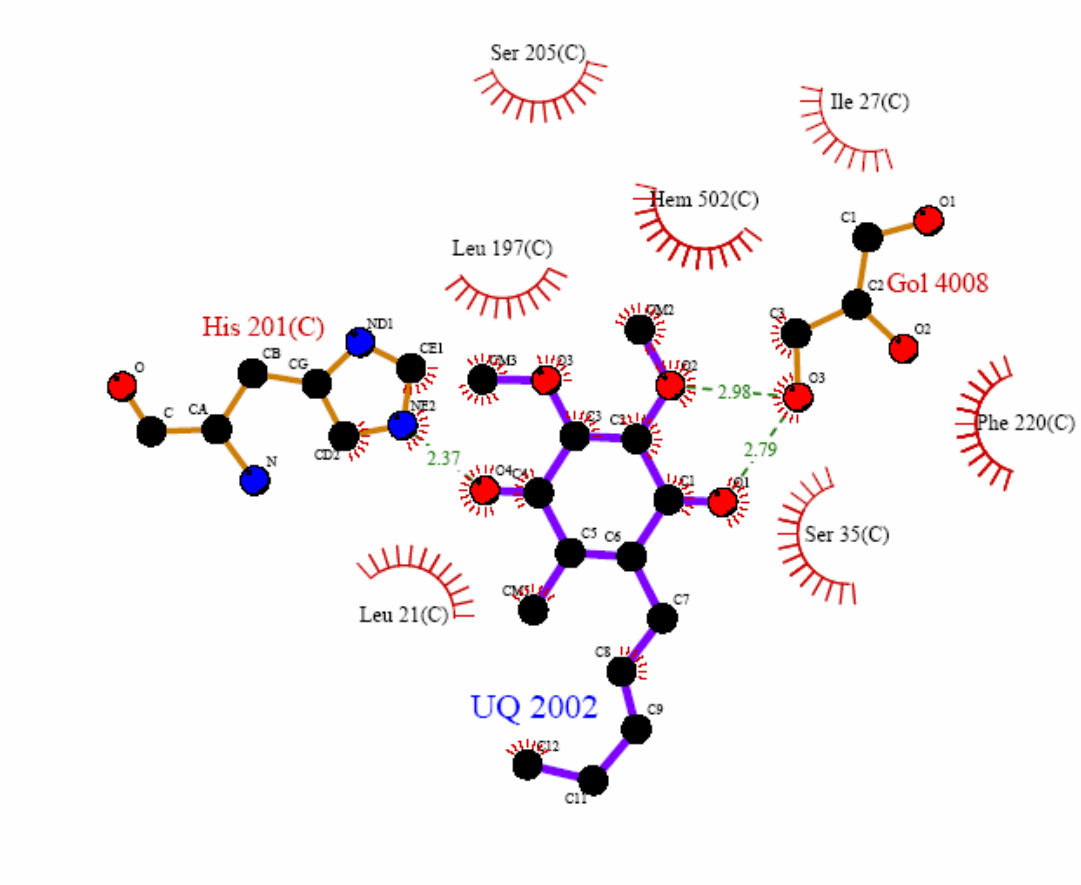

Figure 17. Ubiquinone binding in the Q_i site (pdb code 2a06). Gol 4008 is a glycerol molecule.

Q-cycle

The protonmotive Q-cycle hypothesis is commonly used to describe the way ubiquinol is used twice in proton translocation in the bc_1 complex as shown in figure 18 (17,18). Q-cycle hypothesis consists of a two substrate binding site model, composed of one quinol oxidation (Q_o) site and one quinone reduction (Q_i) site. Bifurcation of electrons comes from a quinol at the Q_o site where the first electron is transferred through ISP and cytochrome c_1 to the soluble electron acceptor cytochrome *c* and the second electron is transferred through hemes b_L and b_H to the Q_i site. Bifurcation of electrons is coupled to the translocation of two protons per molecule of quinol. The oxidized quinol may move to the Q_i site to become reduced. One complete Q cycle will use two molecules of quinol and one molecule of quinone resulting in the production of one quinol molecule along with the translocation of four protons to the positive side of the membrane. After the first crystal structure of the bc_1 complex was solved it was found that the FeS anomalous signal was diminished, this effect was attributed to the mobility of the ISP head domain (8). Later, crystallographic studies revealed the anomalous signal for the FeS cluster in different locations as depicted in figure 19 (9,19).

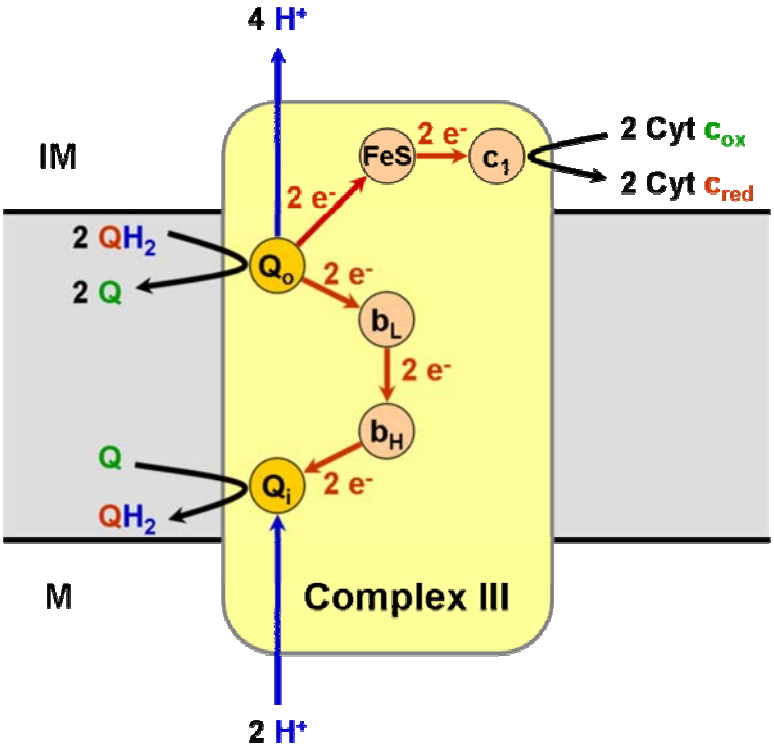

Figure 18. Proton motive Q-Cycle.

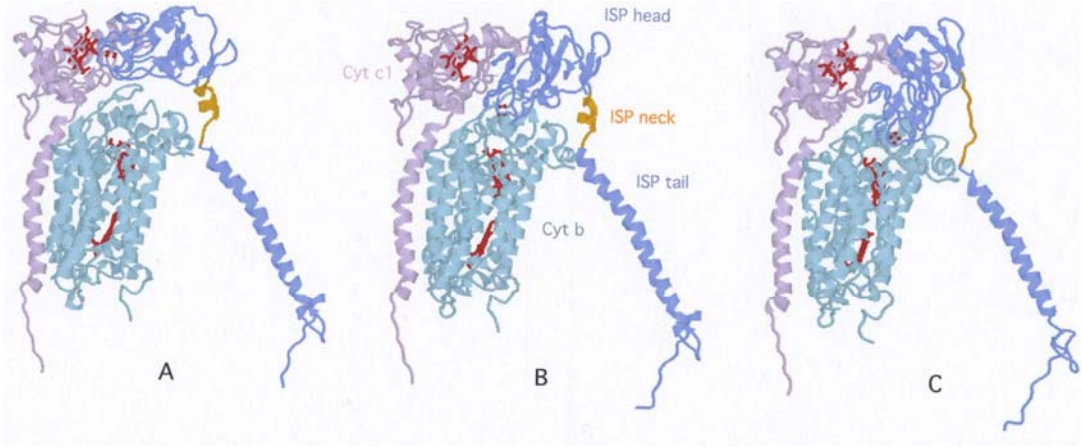

Figure 19. ISP head domain movement. (A) is the ISP_c position, (C) is the ISP_b position and (B) is the loose ISP head domain.

Two noted positions are the position when ISP is docked in the cyt. *b* cavity noted ISP_b and the position of the ISP head domain when the FeS has moved to the cyt. c_1 subunit noted ISP_c. As seen in figure 18 when the ISP_b configuration is present the distance between the FeS and cyt c_1 heme is farther away, and when the ISP_c configuration is present the distance from the FeS to the cyt c_1 heme is much closer. The first electron that's given off in the Q_o site as described by the Q cycle is transferred to FeS in the ISP_b configuration. It was noted in the first solved crystal structure that this distance between FeS and cyt c_1 heme in ISP_b configuration was too far for efficient transfer of the electron from FeS to cyt c_1 heme (8), so it was postulated that it is necessary for the ISP head domain to move to the ISP_c configuration in order to allow for the transfer of the electron from FeS to the cyt c_1 heme. Very well crafted site directed mutagenesis studies provided further evidence to support the notion that mobility of the ISP head domain is needed for proper functioning of the bc_1 complex. It was found that when the region of ISP between the head domain and the membrane bound alpha helix in *Rhodobacter sphaeroides* termed the "neck region" was made more rigid by inserting cysteines to create a disulfide bridge or when neck region residues were mutated to prolines, there was a diminishment of the bc_1 complex activity (20,21). Further mutagenesis studies on ISP and cyt. *b* subunits in *Rhodobacter sphaeroides*, where a double mutant [A185C(cyt. *b*)/K70C(ISP)] was generated to determine whether the head domain movement in head domain of ISP is essential for activity in the bc_1 complex. This double mutant is placed on cyt. *b* and the ISP head domain in a location where the ISP head domain and cyt. *b* come in contact in the ISP_b configuration. The double

mutant revealed that when the di-sulfide bond is formed between the ISP head domain and cyt. *b* (causing the ISP head domain to lock in a fixed position), a diminishment of activity in the bc_1 complex in *Rhodobacter sphaeroides* was observed (22). Similar site directed mutagenesis studies confirmed the bc_1 complex functions as a dimer in solution (23). The combination of x-ray crystallographic structural data and site directed mutagenesis studies provide strong evidence for the importance of the mobility of the ISP head domain in the functioning of the bc_1 complex.

Prior to the first crystal structure of the bc_1 complex, the study of various inhibitors of the bc_1 complex played an important role in elucidating the mechanics of the bc_1 complex (24,25). In spite of intense efforts by many investigators none of the crystal structures of the bc_1 complex show ubiquinol or ubiquinone in the Q_o site as predicted by the Q-cycle. However, some of the crystal structures show various non-competitive inhibitors in the Q_o site.

Another mechanism to describe the functioning of the bc_1 complex has been purposed that consists of the electron taking a linear path from quinol -> b_L -> b_H -> FeS -> c_1 (Figure 20) (26). This linear path mechanism is based off of the observations that in the presences of P side inhibitors myxothiazol, MOA-stilbene, stigmatellin or N-side inhibitor antimycin added to bovine-heart submitochondrial particles (SMP) pretreated with ascorbate and KCN to reduce the high potential components (FeS and cyt c_1 heme) of Complex III, addition of succinate reduced heme b_H followed by a slow and partial reduction of heme b_L (26).

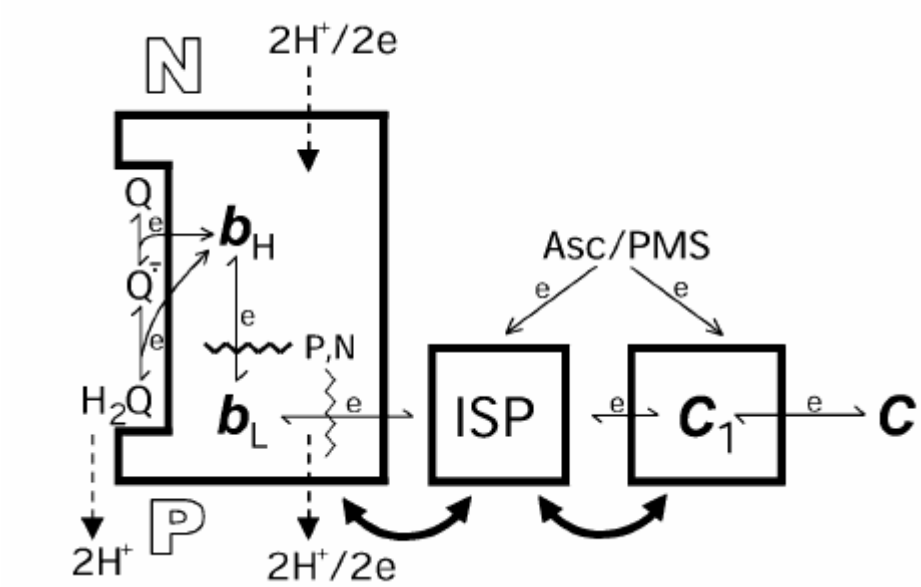

Figure 20. Linear mechanism. Where N is the matrix side and P is the intermembrane space. Asc is ascorbate and PMS is phenazine metho-sulfate.

This is an indication that if the high potential chain (FeS and cyt c_1) were already reduced then the addition of succinate which would cause Complex II to generate a molecule of quinol, and the quinol would then cause the reduction of b_H in complex indication that the first redox group to be reduced in this case is heme b_H contrary to the Q-cycle hypothesis which states that the first redox group to get reduced is the FeS. The linear path mechanism is also based of the observation the reverse electron transfer from ISP reduced with ascorbate plus phenazine metho-sulfate to cytochrome *b* in ubiquinone depleted SMP and ubiquinone replenished SMP revealed that Q was not required for electron transfer from ISP to *b*, a reaction that was inhibited by antimycin (26). The reverse electron transfer experiment is used to argue the lack of the need for a quinone or quinol molecule to allow for the flux of electron flow between cyt. *b* and the high potential chain as described in the proton-motive Q cycle, which would support the conclusion that the electron travels from the heme b_L -> FeS -> c_1. The linear path mechanism also operates off the study that shows that antimycin did not inhibit electron transfer from b_H to ubiquinone, which significantly deviates from the Q-cycle mechanism (26). Several crystal structures show antimycin binding in the Q_i site; if antimycin does not inhibit electron transfer from b_H to quinone then it is possible that an additional binding site for the ubiquinol or ubiquinone substrate exists.

Summary

It is important to note that the protonmotive Q-cycle hypothesis was developed before the first crystal structure of the bc_1 complex was solved, which would have allowed for a more effective analysis of the geometry of the active sites. Considering the resources available at the time of the development of the protonmotive Q-cycle hypothesis, it is astounding to see the predictive power of the Q-cycle hypothesis in effect, now that structural data is available. The Q-cycle hypothesis adequately describes a mechanism for a two separate substrate binding site model in a monomeric bc_1 complex, and these two separate binding sites are also confirmed from the crystal structures with inhibitors for the Q_o and Q_i sites. However, there have not been any experiments to rule out the possibility of more than two binding sites for the substrates in the bc_1 complex. Several studies have opened the door to the recognition of additional substrate binding sites in the bc_1 complex. An intriguing study that was ahead of the studies on the bc_1 complex at its time and before the first crystal structure of the bc_1 complex was solved is the 3-azido-2-methyl-5-methoxy-6-(3,7-dimethyloctyl)1,4-benzoquinone (azido-Q) labeling studies which confirmed the existence of more than two binding sites in the bc_1 complex (27). A study using nuclear magnetic resonance (NMR) recognizes that three molecules of the substrate bind to the bc_1 complex (28). Thus, in order to understand how the bc_1 complex functions correctly, it is critical to have a detailed understanding of the correct number and location of binding sites for the substrates. X-ray diffraction experiments with 2,3,4-trimethoxy-5-decyl-6-methyl-phenol (TMDMP) revealed extremely weak

binding in a third binding site. In order to unambiguously detect and confirm this third binding site 2-Bromo-5,6-dimethoxy-3-pentyl-benzene-1,4-diol (2BrQ), a quinol analogue with bromine substituted in place of the methyl group on quinol, was synthesized.. The bromine anomalous signal in the x-ray diffraction data will be used to allow for the detection of the position and orientation of the active quinol analog. X-ray diffraction data is collected at a wavelength slightly above the bromine edge to allow for the detection of the bromine anomalous signal in the x-ray diffraction data. Preliminary kinetics studies show 2BrQ initially active in the bc_1 complex at lower concentrations and inhibition of the bc_1 complex at higher concentrations. X-ray crystallographic analysis of the bc_1 complex crystals prepared with 2BrQ show an anomalous signal for the bromine in a third substrate binding site separate from the Q_i and Q_o sites described in the Q-cycle model. This binding site is located in the same region as revealed by azido-Q labeling experiments (27). When 2BrQ is combined with 2-(10-Bromo-decyl)-5,6-dimethoxy-3-methyl-benzene-1,4-diol (QC10Br) in bc_1 complex crystals the anomalous signal for the 2BrQ shows up in a new third Q_m binding site and the QC10Br is detectable in the Q_o site. Identifying the 2BrQ molecule in the Q_m binding site allows for an understanding of the binding sequence of substrates in the bc_1 complex due to the 2BrQ binding properties in the when the bc_1 complex is oxidized verses reduced, where the oxidized bc_1 complex would be the state of the enzyme in the beginning of the reaction mechanism. The x-ray crystallographic analysis of the 2BrQ molecule in conjunction with other studies allows for the deciphering of the most probable electron transferring pathways utilized by the bc_1 complex.

REFERENCES

1. Sazanov, L. A., and Hinchliffe, P. (2006) Structure of the Hydrophilic Domain of Respiratory Complex I from *Thermus thermophilus Science* **311**(5766), 1430-1436
2. Horsefield, R., Yankovskaya, V., Sexton, G., Whittingham, W., Shiomi, K., Omura, S., Byrne, B., Cecchini, G., and Iwata, S. (2006) Structural and computational analysis of the quinone-binding site of complex II (succinate-ubiquinone oxidoreductase): a mechanism of electron transfer and proton conduction during ubiquinone reduction *J Biol Chem* **281**(11), 7309-7316
3. Huang, L. S., Borders, T. M., Shen, J. T., Wang, C. J., and Berry, E. A. (2005) Crystallization of mitochondrial respiratory complex II from chicken heart: a membrane-protein complex diffracting to 2.0 A *Acta Crystallogr D Biol Crystallogr* **61**(Pt 4), 380-387
4. Gencic, S., Schagger, H., and von Jagow, G. (1991) Core I protein of bovine ubiquinol-cytochrome-c reductase; an additional member of the mitochondrial-protein-processing family. Cloning of bovine core I and core II cDNAs and primary structure of the proteins *Eur J Biochem* **199**(1), 123-131

5. Deng, K., Shenoy, S. K., Tso, S. C., Yu, L., and Yu, C. A. (2001) Reconstitution of mitochondrial processing peptidase from the core proteins (subunits I and II) of bovine heart mitochondrial cytochrome bc(1) complex *J Biol Chem* **276**(9), 6499-6505

6. Deng, K., Zhang, L., Kachurin, A. M., Yu, L., Xia, D., Kim, H., Deisenhofer, J., and Yu, C. A. (1998) Activation of a matrix processing peptidase from the crystalline cytochrome bc1 complex of bovine heart mitochondria *J Biol Chem* **273**(33), 20752-20757

7. Berry, E. A., Huang, L. S., Saechao, L. K., Pon, N. G., Valkova-Valchanova, M., and Daldal, F. (2004) X-Ray Structure of Rhodobacter Capsulatus Cytochrome bc (1): Comparison with its Mitochondrial and Chloroplast Counterparts *Photosynth Res* **81**(3), 251-275

8. Xia, D., Yu, C. A., Kim, H., Xia, J. Z., Kachurin, A. M., Zhang, L., Yu, L., and Deisenhofer, J. (1997) Crystal structure of the cytochrome bc1 complex from bovine heart mitochondria *Science* **277**(5322), 60-66

9. Iwata, S., Lee, J. W., Okada, K., Lee, J. K., Iwata, M., Rasmussen, B., Link, T. A., Ramaswamy, S., and Jap, B. K. (1998) Complete structure of the 11-subunit bovine mitochondrial cytochrome bc1 complex *Science* **281**(5373), 64-71

10. Berry, E. A., Huang, L. S., Zhang, Z., and Kim, S. H. (1999) Structure of the avian mitochondrial cytochrome bc1 complex *J Bioenerg Biomembr* **31**(3), 177-190

11. Hunte, C., Koepke, J., Lange, C., Rossmanith, T., and Michel, H. (2000) Structure at 2.3 A resolution of the cytochrome bc(1) complex from the yeast *Saccharomyces cerevisiae* co-crystallized with and anti-body Fv fragment *Structure* **15**, 669-684

12. Esser, L., Quinn, B., Li, Y., Zhang, M., Elberry, M., Yu, L., Yu, C. A., and D., X. (2004) Crystallographic studies of quinol oxidation site inhibitors: a modified classification of inhibitors for the cytochrome bc(1) complex. *J Mol Biol* **341**, 281-302

13. Gao, X., Wen, X., Esser, L., Quinn, B., Yu, L., Yu, C. A., and Xia, D. (2003) Structural basis for the quinone reduction in the bc1 complex: a comparative analysis of crystal structures of mitochondrial cytochrome bc1 with bound substrate and inhibitors at the Qi site *Biochemistry* **42**(30), 9067-9080

14. Gao, X., Wen, X., Yu, C., Esser, L., Tsao, S., Quinn, B., Zhang, L., Yu, L., and Xia, D. (2002) The crystal structure of mitochondrial cytochrome bc1 in complex with famoxadone: the role of aromatic-aromatic interaction in inhibition *Biochemistry* **41**(39), 11692-11702

15. Wallace, A C, Laskowski, R A, and Thornton ,J M. (1995) LIGPLOT: A program to generate schematic diagrams of protein-ligand interactions. *Prot. Eng.*, **8**, 127-134.

16. Ohnishi, T., Brandt, U., and von Jagow, G. (1988) Studies on the effect of stigmatellin derivatives on cytochrome b and the Rieske iron-sulfur cluster of cytochrome c reductase from bovine heart mitochondria *Eur J Biochem* **176**(2), 385-389

17. Mitchell, P. (1976) Possible molecular mechanisms of the protonmotive function of cytochrome systems. *J Theor Biol* **62**, 327-367

18. Trumpower, B. L. (1990) The protonmotive Q cycle. Energy transduction by coupling of proton translocation to electron transfer by the cytochrome bc1 complex *J Biol Chem* **265**(20), 11409-11412

19. Zhang, Z., Huang, L., Shulmeister, V. M., Chi, Y. I., Kim, K. K., Hung, L. W., Crofts, A. R., Berry, E. A., and Kim, S. H. (1998) Electron transfer by domain movement in cytochrome bc1 *Nature* **392**(6677), 677-684

20. Tian, H., Yu, L., Mather, M. W., and Yu, C. A. (1998) Flexibility of the neck region of the rieske iron-sulfur protein is functionally important in the cytochrome bc1 complex *J Biol Chem* **273**(43), 27953-27959

21. Tian, H., White, S., Yu, L., and Yu, C. A. (1999) Evidence for the head domain movement of the rieske iron-sulfur protein in electron transfer reaction of the cytochrome bc1 complex *J Biol Chem* **274**(11), 7146-7152

22. Xiao, K., Yu, L., and Yu, C. A. (2000) Confirmation of the involvement of protein domain movement during the catalytic cycle of the cytochrome bc1 complex by the formation of an intersubunit disulfide bond between cytochrome b and the iron-sulfur protein *J Biol Chem* **275**(49), 38597-38604

23. Xiao, K., Chandrasekaran, A., Yu, L., and Yu, C. A. (2001) Evidence for the intertwined dimer of the cytochrome bc(1) complex in solution *J Biol Chem* **276**(49), 46125-46131

24. Link, T. A., Haase, U., Brandt, U., and von Jagow, G. (1993) What information do inhibitors provide about the structure of the hydroquinone oxidation site of ubihydroquinone: cytochrome c oxidoreductase? *J Bioenerg Biomembr* **25**(3), 221-232

25. von Jagow, G., and Link, T. A. (1986) Use of specific inhibitors on the mitochondrial bc1 complex *Methods Enzymol* **126**, 253-271

26. Matsuno-Yagi, A., and Hatefi, Y. (1999) Ubiquinol:cytochrome c oxidoreductase. Effects of inhibitors on reverse electron transfer from the iron-sulfur protein to cytochrome b *J Biol Chem* **274**(14), 9283-9288

27. He, D. Y., Yu, L., and Yu, C. A. (1994) Ubiquinone binding domains in bovine heart mitochondrial cytochrome b *J Biol Chem* **269**(3), 2292-2298

28. Bartoschek, S., Johansson, M., Geierstanger, B. H., Okun, J. G., Lancaster, C. R., Humpfer, E., Yu, L., Yu, C. A., Griesinger, C., and Brandt, U. (2001) Three molecules of ubiquinone bind specifically to mitochondrial cytochrome bc1 complex *J Biol Chem* **276**(38), 35231-35234

CHAPTER II

X-ray Diffraction Analysis of TMDMP, a Non-oxidizable Ubiquinol Analogue that Binds to the bc_1 Complex

ABSTRACT

The bc_1 complex in the electron transfer chain plays a critical role in the production of energy for aerobic cells. The currently accepted proton motive Q-cycle hypothesis is used to describe the catalytic mechanism for the bc_1 complex. The Q-cycle purposes two binding sites. The two binding sites are the Q_o site, for the oxidation of quinol, and the Q_i binding site, for the reduction of quinone. The location of the Q_o site is currently the same location as known non-competitive inhibitors like stigmatellin. To determine a more accurate depiction of the Q_o site, TMDMP was synthesized. TMDMP is a competitive inhibitor that is structurally similar to quinol and we are able to detect the position of TMDMP in a third binding site. By mimicking the reducing effect of quinol on the bc_1 complex with TMDMP, three different binding states for TMDMP were revealed. By using a highly structurally similar substrate analog in combination with the injection of electrons into the complex, allowed for the ability to follow important substrate positions in the complex by the use of macromolecular x-ray crystallography, which has proven in this case to be a desired alternative when time-resolved crystallography techniques are not feasible. From these results a dual quinol oxidation site Q-cycle mechanism may exist, where it may be possible that quinol oxidation would occur in two separate binding sites.

INTRODUCTION

Ninety percent of the energy needed for aerobic cells comes from the mitochondria respiratory chain by way of ATP synthesis. The respiratory chain contains four electron transfer complexes and an ATP synthase (1). Ubiquinol-cytochrome-c oxidoreductase (bc_1 complex) is a dimeric transmembrane protein that is the central segment of the respiratory chain in the mitochondria. The bc_1 complex oxidizes ubiquinol and reduces cytochrome *c* with concomitant generation of a proton gradient and membrane potential for ATP synthesis by ATP synthase (2).
The mitochondria bc_1 complex is a dimer with a molecular mass of about 500 kDa. Three subunits out of eleven total subunits are essential for electron transfer. The three essential subunits are cytochrome *b* which contains a total two *b*-type hemes (b_l and b_h), cytochrome c_1 which contains a *c*-type heme, and iron-sulfur protein (ISP) which contains a 2Fe-2S (FeS) cluster.

The protonmotive Q-cycle hypothesis is commonly used to describe the way ubiquinol is used twice in proton translocation in the bc_1 complex (3,4). The Q-cycle hypothesis describes two substrate binding sites, a quinol oxidation (Q_o) site and a quinone reduction (Q_i) site. Bifurcation of electrons comes from a quinol at the Q_o site where the first electron is transferred through ISP and cytochrome c_1 to the soluble electron acceptor cytochrome *c* and the second electron is transferred through hemes b_L and b_H to the Q_i site. The bifurcation of electrons is coupled to the translocation of two protons per molecule of quinol. The reduced quinol may move to the Q_i site to become oxidized. One complete Q cycle will use two molecules of

quinol and produce one quinol molecule along with the translocation of four protons to the positive side of the membrane.

The first crystal structure of cytochrome bc_1 complex from bovine heart mitochondria was solved at 2.9 Å resolution in 1997 (5). A year later more complete structures were reported (6-8). None of the crystal structures of the bc_1 complex show quinol or quinone in the Q_o site. However, some of the crystal structures show various non-competitive inhibitors in the Q_o site (9). The key feature of the Q-cycle mechanism is the initial bifurcation of electrons from ubiquinol in the Q_o site. Thus, in order to understand how the bc_1 complex functions correctly, it is critical to have a detailed understanding of the correct binding site/sites of the substrate.

In order to locate the initial binding site for quinol, 2,3,4-Trimethoxyl-decyl-methyl-phenol (TMDMP) was synthesized and kinetic studies show TMDMP to be a competitive inhibitor as opposed to the non-competitive inhibitors previously used to define the initial quinol binding site (10). TMDMP is almost identical to quinol except for the substitution of a methoxy group in place of the hydroxyl group as shown in figure 1. Because TMDMP is a competitive inhibitor and is highly structurally similar to ubiquinol, the TMDMP binding site should provide compelling evidence for the initial binding site of ubiquinol. We are able to detect the TMDMP binding site by x-ray crystallography. The initial binding site for this competitive inhibitor is different from the binding site of the other inhibitors. This initial binding site of TMDMP will be referred to as Q_m, the "m" is used to indicate middle. The Q_m binding site is located more toward the middle of the membrane relative to the Q_o and

Q_i sites. The detection of the possible initial substrate binding site will allow for a more in-depth and complete understanding of how the bc_1 complex functions.

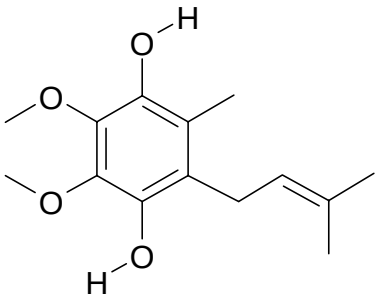

A. Quinol with one isoprene unit.

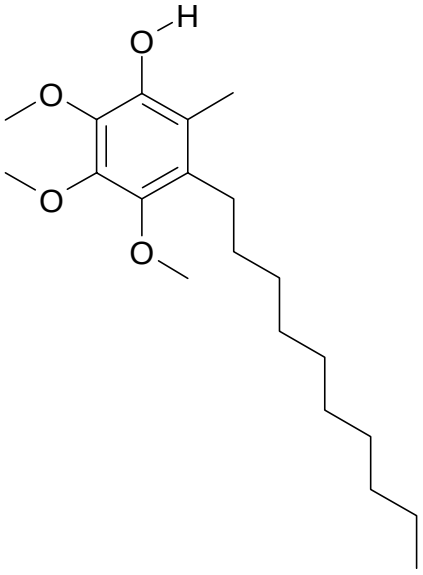

B. TMDMP

Figure1. Structure of quinol with one isoprene unit and TMDMP

MATERIAL AND METHODS

Protein preparation and crystallization.

The bc_1 complex from bovine heart mitochondria was prepared as described previously (5,11). For crystallization, the bc_1 particles were subject to an additional 15-step NH_4Ac fractionation to remove impurities; pure bc_1 complex in the oxidized form was recovered from the precipitates formed between 18.5% and 33.5% NH_4Ac saturation; and the final product was dissolved in 50 mM Tris-HCl buffer, pH 7.8, containing 0.66 M sucrose to a protein concentration of 30 mg/ml and frozen at -80 ˚C until use. The concentrations of cyt. *b* and c_1 were determined spectroscopically, using millimolar extinction coefficients of 28.5 and 17.5 for cyt. *b* and c_1, respectively. The homogeneity in redox state of bc_1 was confirmed spectrophotometrically.

Purified bc_1 complexes were adjusted to a final concentration of 20 mg/ml in a solution containing 50 mM MOPS buffer at pH 7.2, 20 mM ammonium acetate, 20% (w/v) glycerol, and either 0.1% of decanoyl-N-methylglucamide or 0.1% of diheptanoyl phosphatidylcholine or 0.16% sucrose monocaprate. Native crystals were grown in either sitting or hanging drops and appeared in 3-4 weeks. The TMDMP bound bc_1 crystals were grown under similar conditions except that a five-fold in molar excess of TMDMP was added to the protein solution prior to crystallization. Both native and TMDMP bound bc_1 crystals had a rectangular shape ranging in sizes from 0.4 to 0.7 mm, and were cryo-protected at a glycerol

concentration of 30-40%. The TMDMP bound crystals had the same space group and similar unit cell dimensions to that of native crystals.

X-ray diffraction data collection and reduction.

Crystals were stable at synchrotron radiation sources when cryo-cooled to 100 K, allowing collection of complete data sets. Data were collected at beamlines IMCA-CAT and SBC-CAT of the Argonne Photon Source at Argonne National Laboratory in Argonne IL., with a wavelength of 1.0 Å. Raw diffraction data were processed with DENZO, and integrated intensities were merged and scaled with SCALEPACK, both are part of the HKL program package (12).

Data analysis, structure refinement and modeling.

The CNS software package (13) were used for merging and scaling different data sets, calculating structure factors from atomic models, density modifications and computing Fourier maps. The atomic coordinates of the native bc_1 (5)(8) were used to initially phase the data followed by rigid body refinement. Xfit (14), Molscript and Raster3D were used for atomic modeling and molecular graphic presentation.

RESULTS AND DISCUSSION

TMDMP binding in oxidized bc_1 complex crystals

The bc_1 complex inhibitor binding sites are located in the cytochrome *b* subunit. Cytochrome *b* consists of eight transmembrane helixes that are labeled sequentially from A to H starting from the N-terminus. Currently, there are only two binding sites used to describe the Q-cycle mechanism. One of the binding sites is the quinol oxidation site, located where the inhibitor stigmatellin binds and the other is the quinone reduction site located where the inhibitor antimycin binds. The initial binding site for TMDMP is located in a third binding site separate from the two binding sites used to describe the Q cycle mechanism. The initial binding site for TMDMP, in mostly oxidized bc_1 complex crystals, became visible in a difference electron density map ($F_o^{TMDMP} - F_o^{Native}$ 3.7 Å) and shows a 6.85 sigma peak for TMDMP in the third binding site labeled Q_m and no detectable peaks show up in the Q_o site. The position of TMDMP in the Q_m site relative to the position of stigmatellin and antimycin in the Q_o site can be seen in figure 2. This mostly oxidized binding state will be referred to as T_1. Residues (F325, W326, V329, L333 and T336) of helix G and residues (M96, Y95, and I92) of helix D surround the cavity opening for the Q_m binding site. The interior of the Q_m binding site is defined by residues (Y358, I362, L332, L328) on the right side of the cavity, residues (Y195, L120, V98) on the left side of the cavity, residue (F276) on the top of the cavity, residues (I304, L102) on the bottom of the cavity and residue (L301) located deep in the interior back of the cavity.

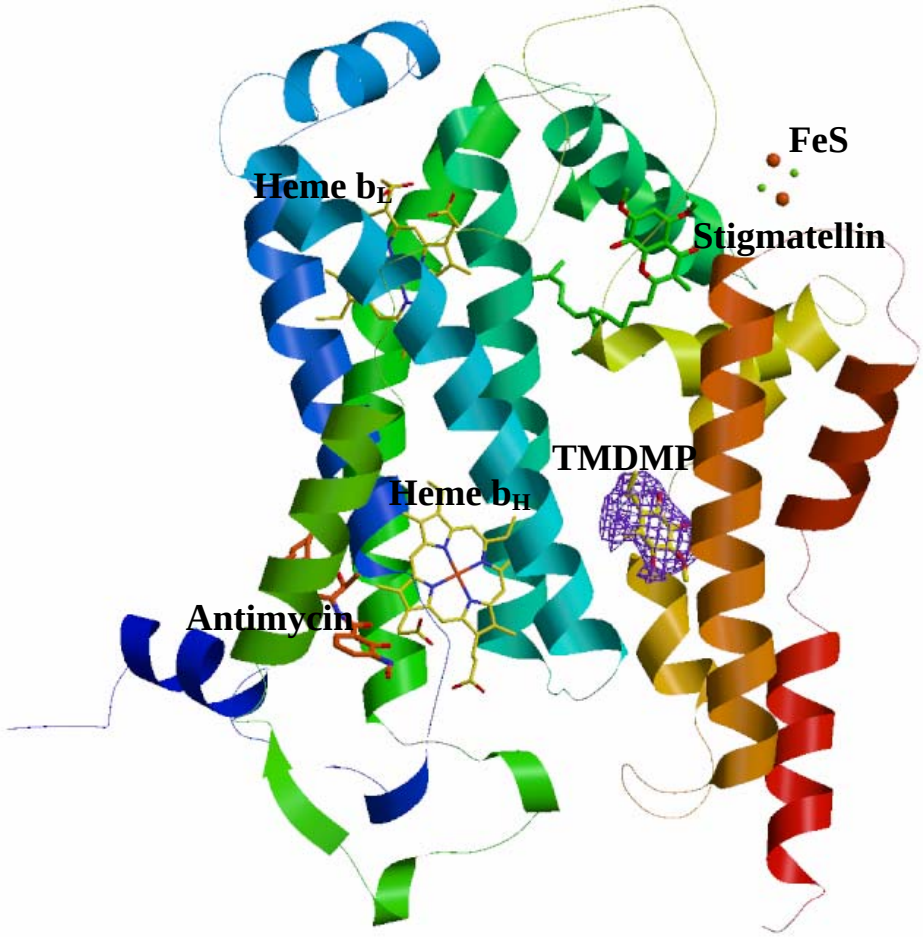

Figure 2. Inhibitors and difference map density in the T_1 state. The density is contoured at 4 σ.

Preliminary molecular modeling analysis alludes to the possibility of hydrogen bonding between Y358 and the substrate (Figure 3). The position of TMDMP is closer to heme b_H (about 7.02 angstroms to atom CBC on heme b_H) than it is to heme b_L (about 15.96 angstroms to the CBC atom on heme b_L). TMDMP density is about 25 angstroms away from the FeS cluster position when the FeS cluster is in the position directly above cytochrome *b* or the "b-position". Since we see the initial binding of TMDMP, a competitive inhibitor, closest to heme b_H, it is possible that heme b_H would receive the first electron from quinol in this binding site.

TMDMP binding in reduced bc_1 complex crystals

From the oxidized crystals we are able to determine the initial binding site location for TMDMP. One very important property of quinol is its ability to reduce the bc_1 complex. In order to investigate what happens after quinol enters the Q_m site, it is important to simulate the reducing effect that quinol has on the bc_1 complex after it enters the Q_m site. By employing a technique where bc_1 crystals with TMDMP were reduced either before or after crystal growth, allowed for the ability to simulate the reducing effect that quinol has on the bc_1 complex. By reducing crystals after crystal growth, we are able to take advantage of the greatly diminished rotational and translational degrees of freedom of the bc_1 complex, which may affect a weakly binding intermediate. Reduction after crystal growth also has an effect on the FeS occupancy. These characteristics appear to have significant ramifications on the binding affinity properties of TMDMP and reveal important insights into the quinol oxidation in the bc_1 complex.

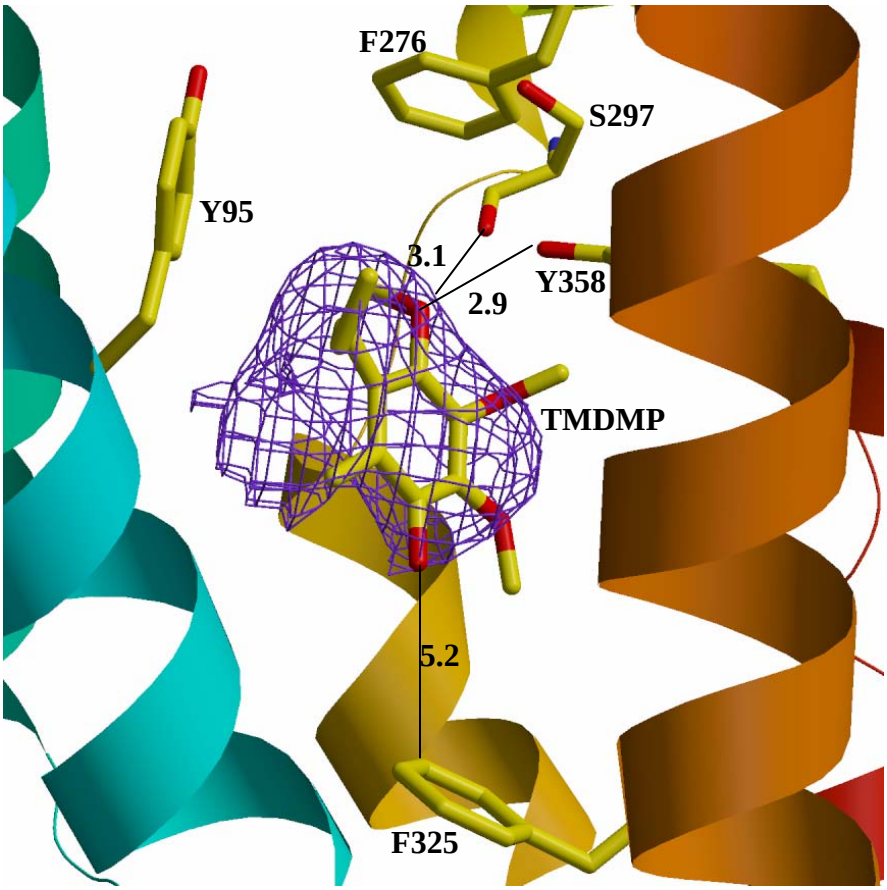

Figure 3. T_1 state close up.

Mostly oxidized bc_1 crystals were grown with excess TMDMP, then after crystal growth the oxidized crystals were then soaked with ascorbate, at 4 times cytochrome *c* concentration, to reduce the crystals. Surprisingly, a difference electron density map ($F_o^{TMDMP} - F_o^{Native}$ 3.6 Å) reveals the binding of three TMDMP molecules. There are two peaks in the Q_m site with sigma values of 5.65 and 6.60 and one peak in the Q_o site at 5.61 sigma (Figure 4). We shall refer to this binding state as T_2. It appears from the peak height values for the Q_m site that the molecule representing the 5.65 peak has a weaker affinity for the binding site. This is in agreement with the notion of a strong binding (Q_{oS}) and weak binding (Q_{oW}) substrate (21). Interestingly enough the Q_{oS} peak is closer to Y358, alluding to the possibility that the hydrogen bonding with the hydroxyl group of Y358 may account for the stronger binding affinity. The two TMDMP molecules in the Q_m site are clearly resolved in a 5 sigma contoured density map as seen in figure 5. The residues surrounding the peak in the Q_o site are V145, I146, L149, I268, P270, F274, Y278, L281 and L294. The peak that resides in the Q_o site appears to overlap the position of stigmatellin and other Q_o site inhibitors (Figure 6). We see from the position of the peak that Y278 may play a role in parallel-displaced pi stacking interactions with the substrate. Parallel-displaced pi stacking interactions are interactions that involve pairs (dimers) of aromatic rings in an off-centered parallel orientation. Aromatic-aromatic interactions have been shown to be important for inhibitor binding in the bc_1 complex (15).

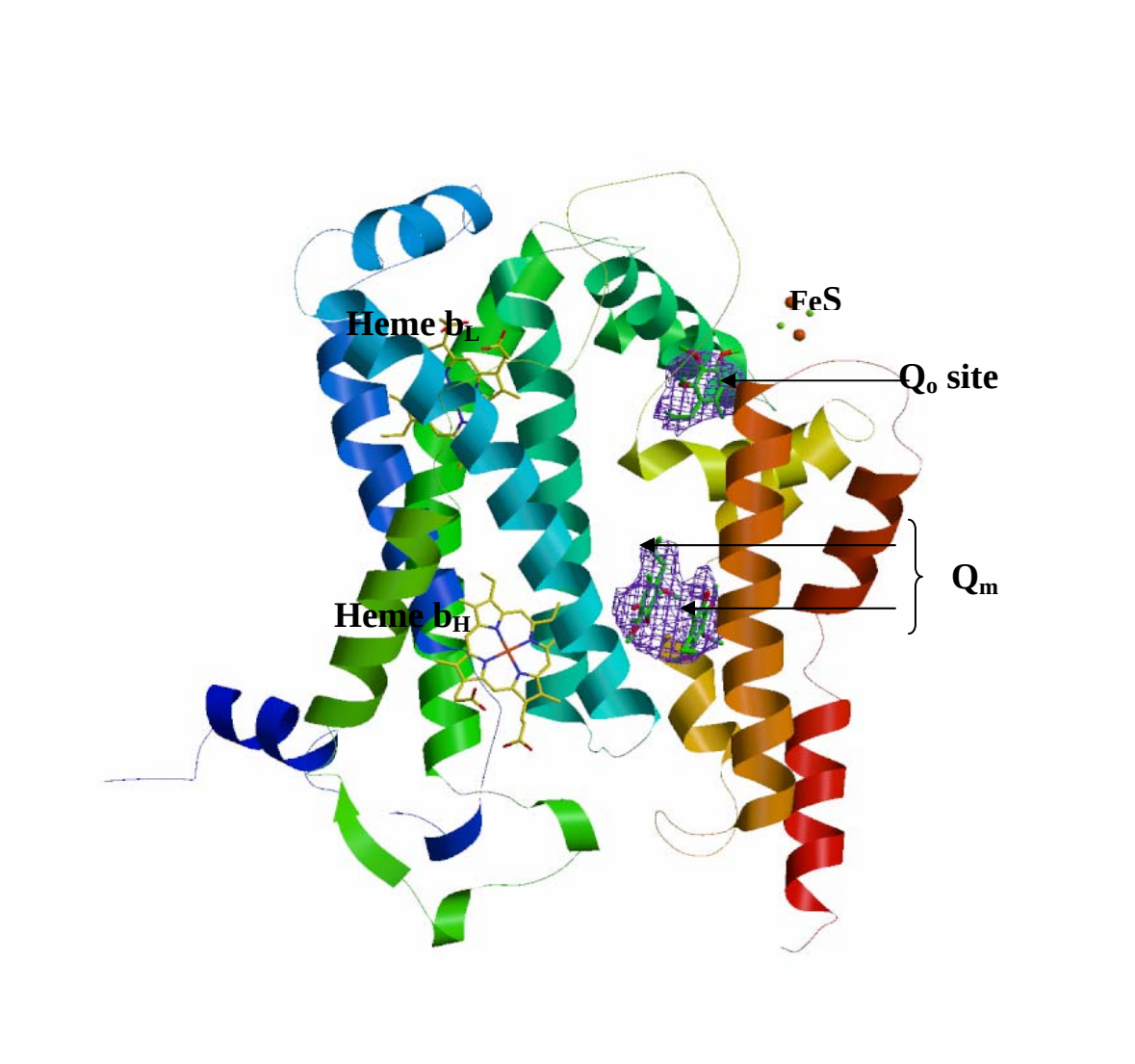

Figure 4. T_2 state TMDMP binding in both Q_o and Q_m sites.

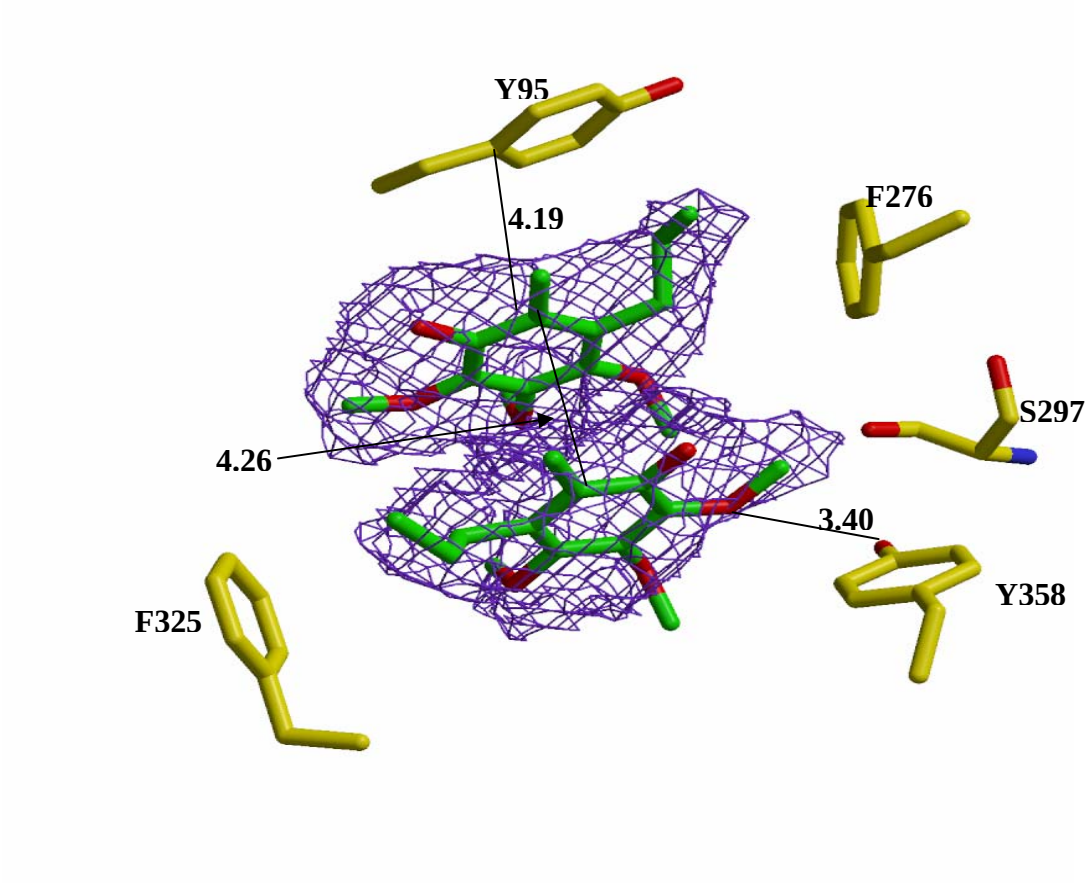

Figure 5. T_2 TMDMP close up of Q_m site. Distances are in angstroms.

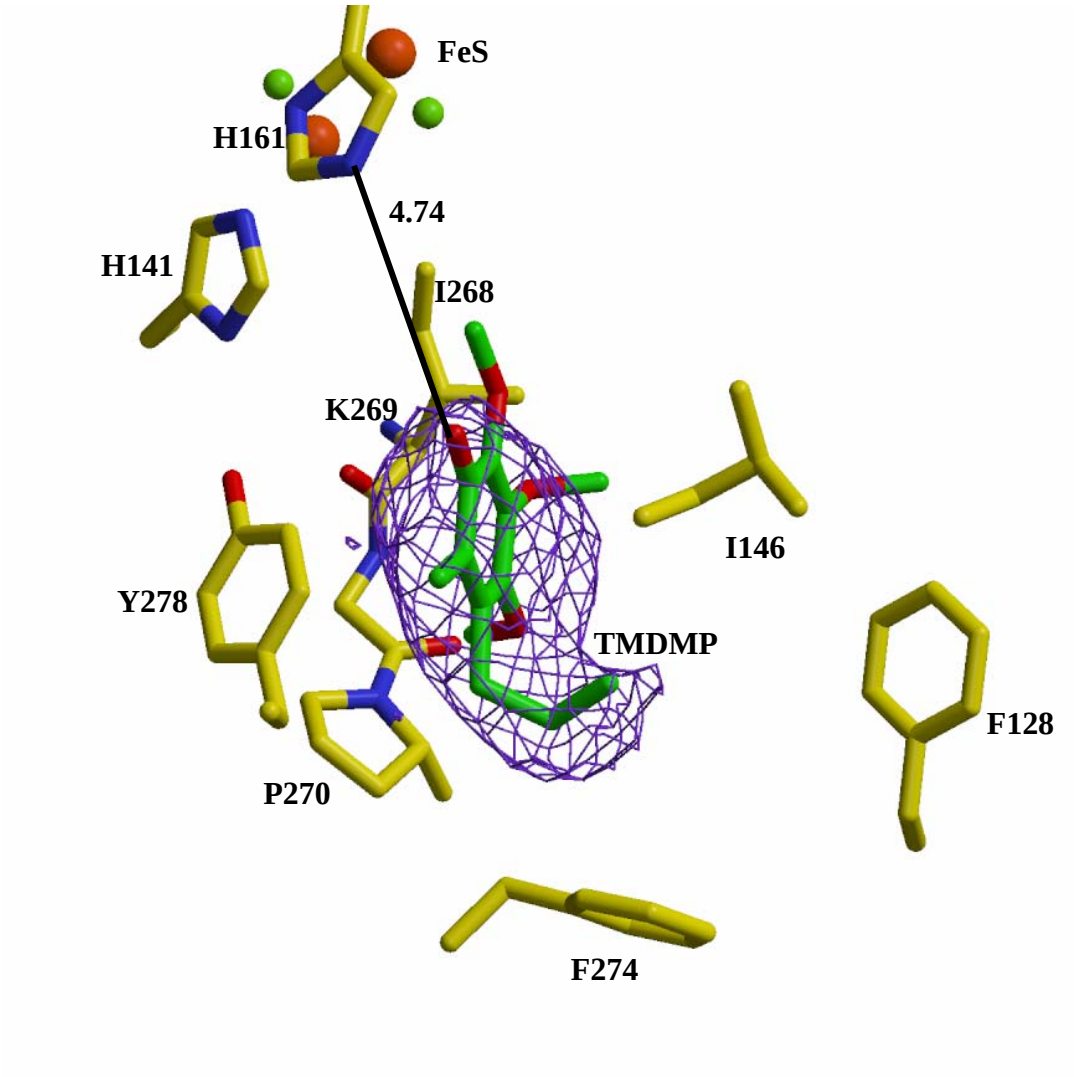

Figure 6. T_2 TMDMP close up of Q_o site. Distance is in angstrom.

When the reduction occurred before crystal growth of the bc_1 complex and TMDMP, a difference electron density map [$F_o^{TMDMP} - F_o^{Native}$ 4.5 Å] shows a 5.9 sigma peak in the Q_o site and density less than 2 sigma in the Q_m site. This state will be referred to as T_3. It seems probable that the increased rotational and translational degrees of freedom for the bc_1 complex may be necessary to facilitate the release of the Q_m site molecules. In the Q_o site we see that the peak has moved farther inside the site somewhat overlapping the other ring moiety of stigmatellin (Figure 7). A comparison of TMDMP in the Q_o site for T_2 and T_3 can be seen in figure 8. It may be possible that each of the ring moieties of stigmatellin may indeed represent important transition state positions for the substrate. Solid state NMR studies using ^{13}C-labelled quinone, show that the binding of myxothiazol (a Q_o site inhibitor) allowed for the displacement of ~ 2.28 mole of quinone / mole bc_1 (16). This was however attributed to the hypothetical and remote possibility of myxothiazol having weak affinity for the Q_i site. It may be possible that myxothiazol displaced the quinone in the Q_o site and the Q_m site. Stigmatellin was shown to displace close to two quinone molecules, which may have been the quinone in the Q_o site and Q_m site. Photo-affinity labeling experiments are also in agreement with the Q_o and Q_m sites. Photo-affinity labeling using [^{3}H]azido-Q shows labeling on two sites, residues 326-336 which would correspond to the Q_m cavity and residues 142-155 which would correspond to the Q_o cavity (17). The position of these two photo-affinity labeled sites relative to TMDMP and stigmatellin are shown in (Figure 9).

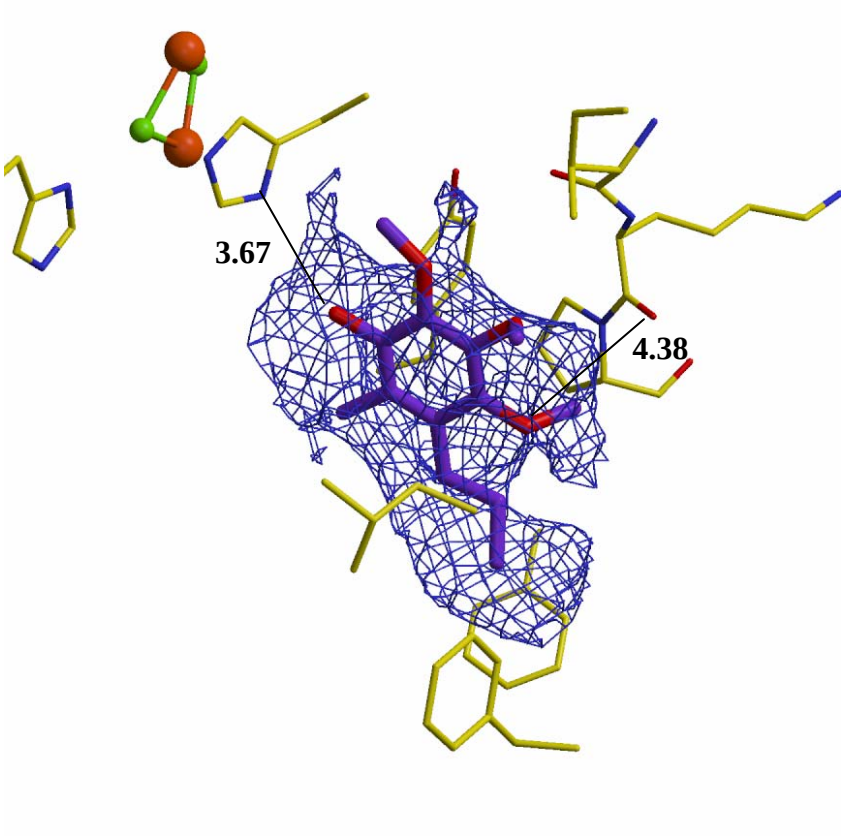

Figure 7. T_3 TMDMP binding in the Q_o site. Distance is in angstroms.

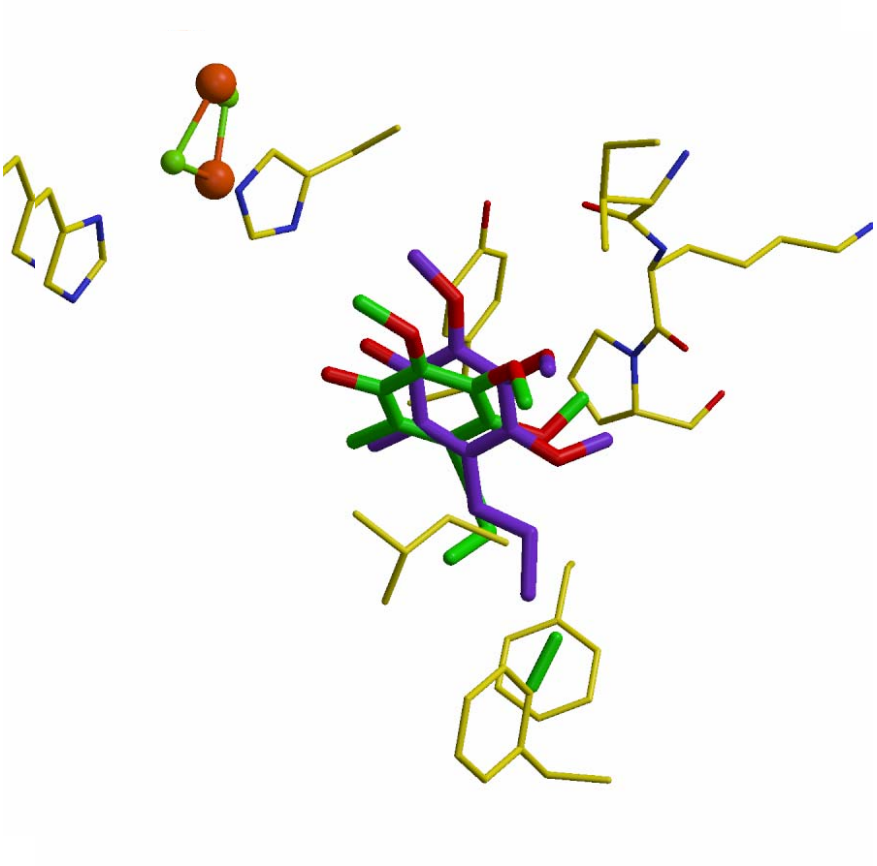

Figure 8. Comparison of T_2 (green) and T_3 (blue) in the Q_o site. To outside of the cavity is to the left of the figure.

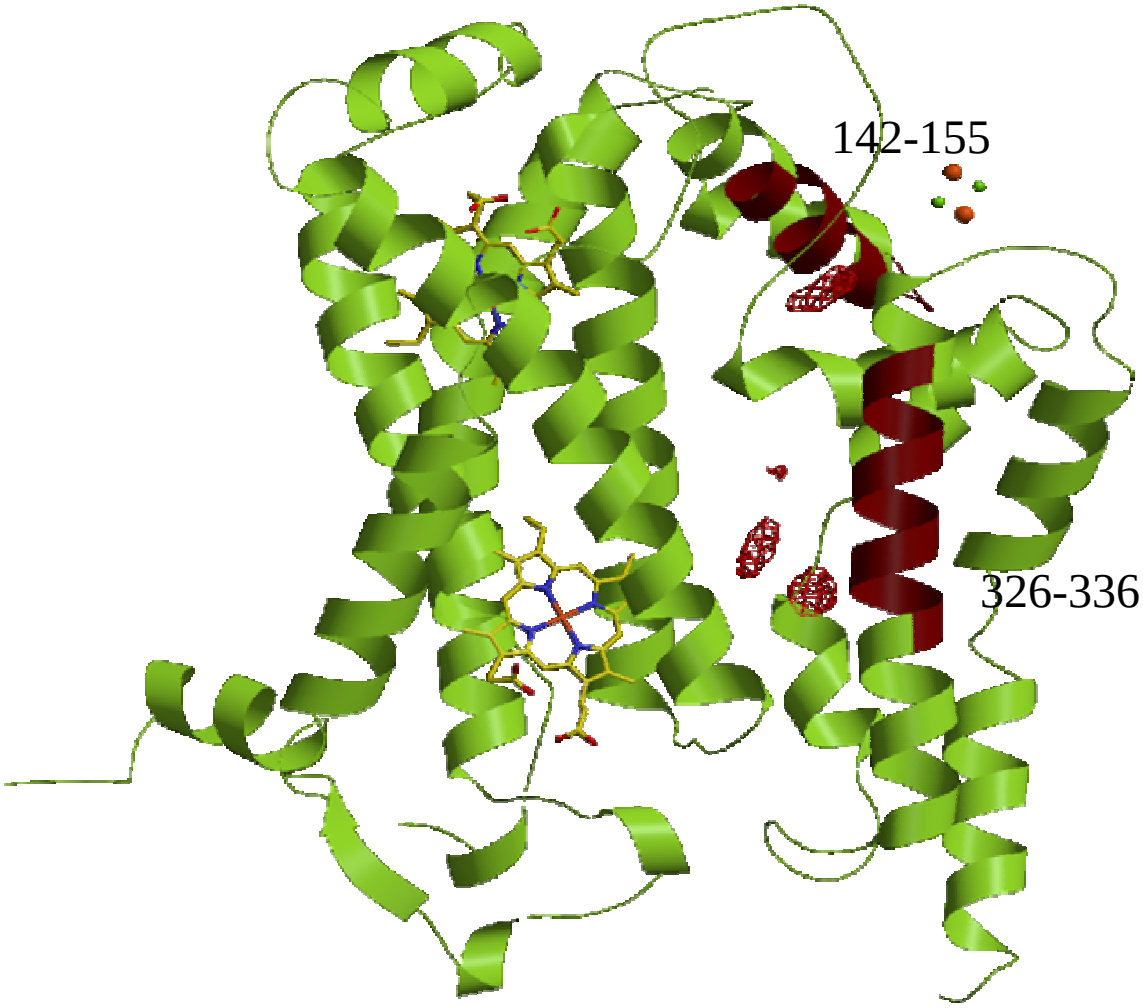

Figure 9. Azido Q Labeling. Red density is T_2 difference map contoured at 5 sigma. Residues that were within the fragment found to be labeled by azido-Q are colored in red.

FeS occupancy in oxidized vs. reduced

The iron sulfur cluster occupancy in the T_1 state appears to be significantly diminished relative to the T_3 state where we observe a stronger signal. It has been shown previously from native bc_1 complex crystals that the occupancy of the FeS cluster in the b position is sensitive to the reduction state of the bc_1 complex from anomalous peak height measurements (18). To calculate the normalized FeS cluster peak height we divided the peak height of the FeS cluster by the peak height of the Fe atom in heme b_H. For the T_1, T_2 and T_3 crystals we see normalized peak heights of 0.309, 0.392 and 0.533 respectively for the FeS cluster. In the T_3 crystal it may be that both cytochome c_1 is reduced and heme b_H is slightly reduced. The FeS anomalous peak heights indicate that when the substrate initially binds to the oxidized bc_1 complex in the T_1 state, the iron sulfur cluster has a very low occupancy in the b-position.

Proton motive Q cycle

The essential backbone of the current Q cycle is the initial bifurcation of electrons upon the entry of the first molecule of quinol into the active site of the bc_1 complex. The first electron is hypothesized to go to the high potential iron sulfur cluster and the second electron going to the low potential heme b_L. The initial reduction of heme b_H has previously been purposed where the electron would take a linear path from quinol -> b_H -> b_L -> ISP -> c_1 (19). This linear path however would not take into account the T_2 and T_3 states where you could have direct electron transfer to ISP from quinol thus bypassing hemes b_H and b_L. By being able to see the T_1, T_2, and T_3 states a dual quinol oxidation site Q cycle model may be purposed. From the T_1 state we see that

it is likely that heme b_H is reduced first and interestingly enough, located in the Q_m binding site in the yeast bc_1 complex (pdb code 1ezv) is a crystallographic defined water molecule adjacent to Y359 in yeast cytochrome *b* subunit, which corresponds to Y358 in bovine. This water molecule appears to be the only water molecule assigned in the middle of the membrane, considering the interior of the membrane is indeed hydrophobic it seems plausible that this water molecule may play a role in the reaction mechanism in the Q_m site.

In summary, a viable catalytic mechanism may actually be a combination of linear and bifurcation electron transfer steps. Where the linear step would occur before the bifurcation step, since the Q_m site is closer to heme b_H. Crystallographic refinement and site directed mutagenesis research is in progress to provide a detailed description of the catalytic mechanism inside the active sites of the bc_1 complex.

REFERENCES

1. Hatefi, Y. (1985) The mitochondrial electron transport and oxidative phosphorylation system *Annu Rev Biochem* **54**, 1015-1069
2. Trumpower, B. L. (1990) Cytochrome bc1 complexes of microorganisms *Microbiol Rev* **54**(2), 101-129
3. Trumpower, B. L. (1990) The protonmotive Q cycle. Energy transduction by coupling of proton translocation to electron transfer by the cytochrome bc1 complex *J Biol Chem* **265**(20), 11409-11412
4. Mitchell, P. (1976) Possible molecular mechanisms of the protonmotive function of cytochrome systems. *J Theor Biol* **62**, 327-367
5. Xia, D., Yu, C. A., Kim, H., Xia, J. Z., Kachurin, A. M., Zhang, L., Yu, L., and Deisenhofer, J. (1997) Crystal structure of the cytochrome bc1 complex from bovine heart mitochondria *Science* **277**(5322), 60-66
6. Zhang, Z., Huang, L., Shulmeister, V. M., Chi, Y. I., Kim, K. K., Hung, L. W., Crofts, A. R., Berry, E. A., and Kim, S. H. (1998) Electron transfer by domain movement in cytochrome bc1 *Nature* **392**(6677), 677-684
7. Iwata, S., Lee, J. W., Okada, K., Lee, J. K., Iwata, M., Rasmussen, B., Link, T. A., Ramaswamy, S., and Jap, B. K. (1998) Complete structure of the 11-subunit bovine mitochondrial cytochrome bc1 complex *Science* **281**(5373), 64-71

8. Hunte, C., Koepke, J., Lange, C., Rossmanith, T., and Michel, H. (2000) Structure at 2.3 A resolution of the cytochrome bc(1) complex from the yeast *Saccharomyces cerevisiae* co-crystallized with and anti-body Fv fragment *Structure* **15**, 669-684
9. von Jagow, G., and Link, T. A. (1986) Use of specific inhibitors on the mitochondrial bc1 complex *Methods Enzymol* **126**, 253-271
10. Zhang, L., Li, Z., Quinn, B., Yu, L., and Yu, C. A. (2002) Nonoxidizable ubiquinol derivatives that are suitable for the study of the ubiquinol oxidation site in the cytochrome bc1 complex *Biochim Biophys Acta* **1556**(2-3), 226-232
11. Yu, C. A., and Yu, L. (1980) Resolution and reconstitution of succinate-cytochrome c reductase: preparations and properties of high purity succinate dehydrogenase and ubiquinol-cytochrome c reductase *Biochim Biophys Acta* **591**(2), 409-420
12. Minor, W., Tomchick, D., and Otwinowski, Z. (2000) Strategies for macromolecular synchrotron crystallography *Structure* **8**(5), R105-110
13. Brunger, A. T., Adams, P. D., Clore, G. M., DeLano, W. L., Gros, P., Grosse-Kunstleve, R. W., Jiang, J. S., Kuszewski, J., Nilges, M., Pannu, N. S., Read, R. J., Rice, L. M., Simonson, T., and Warren, G. L. (1998) Crystallography & NMR system: A new software suite for macromolecular structure determination *Acta Crystallogr D Biol Crystallogr* **54**(Pt 5), 905-921
14. McRee, D. E. (1999) XtalView/Xfit--A versatile program for manipulating atomic coordinates and electron density *J Struct Biol* **125**(2-3), 156-165

15. Gao, X., Wen, X., Yu, C., Esser, L., Tsao, S., Quinn, B., Zhang, L., Yu, L., and Xia, D. (2002) The crystal structure of mitochondrial cytochrome bc1 in complex with famoxadone: the role of aromatic-aromatic interaction in inhibition *Biochemistry* **41**(39), 11692-11702
16. Bartoschek, S., Johansson, M., Geierstanger, B. H., Okun, J. G., Lancaster, C. R., Humpfer, E., Yu, L., Yu, C. A., Griesinger, C., and Brandt, U. (2001) Three molecules of ubiquinone bind specifically to mitochondrial cytochrome bc1 complex *J Biol Chem* **276**(38), 35231-35234
17. He, D. Y., Yu, L., and Yu, C. A. (1994) Ubiquinone binding domains in bovine heart mitochondrial cytochrome b *J Biol Chem* **269**(3), 2292-2298
18. Yu, C. A., Wen, X., Xiao, K., Xia, D., and Yu, L. (2002) Inter- and intra-molecular electron transfer in the cytochrome bc(1) complex *Biochim Biophys Acta* **1555**(1-3), 65-70
19. Matsuno-Yagi, A., and Hatefi, Y. (2001) Ubiquinol:cytochrome c oxidoreductase (complex III). Effect of inhibitors on cytochrome b reduction in submitochondrial particles and the role of ubiquinone in complex III *J Biol Chem* **276**(22), 19006-19011

CHAPTER III

The Detection and Conformation of a Hidden Substrate Binding Site in the bc_1 Complex by the Use of X-ray Crystallographic Anomalous Signal Tracking

ABSTRACT

The bc_1 complex is an integral component of the electron transfer chain responsible for aiding in the production of a proton gradient for ATP synthesis. Mutations in the bc_1 complex are associated with epilepsy and other human diseases. Functioning of the bc_1 complex is commonly explained by the well known proton motive Q cycle. The proton motive Q cycle hypothesis makes use of only two completely separate substrate binding sites in the bc_1 complex. Crystallographic anomalous signal tracking allowed for the deciphering of a hidden third substrate binding site which may have possible implications on the electron transferring pathway in the bc_1 complex.

INTRODUCTION

The electron transfer chain is one of the most exciting aspects of the metabolic process that is essentially important for the aerobic metabolic process. Four electron transfer complexes and an adenosine tri-phosphate (ATP) synthase complex make up the electron transfer chain, which efficiently generates about ninety percent of the energy needed for survival of the organism. Mitochondrial ubiquinol cytochrome *c* oxido-reductase (bc_1 complex) is the central components of the electron transfer chain in the mitochondria. Mutations in the cytochrome bc_1 complex have been found to be related to human diseases (1-4).

The bovine mitochondrial bc_1 complex is a dimeric transmembrane protein that consists of 11 subunits with a dimeric molecular weight of about 500 kDa (5). An intricate electron transfer pathway is used by the bc_1 complex to oxidize ubiquinol and reduces cytochrome *c* with the concomitant generation of a proton gradient and membrane potential for ATP synthesis by ATP synthase. Three subunits out of the eleven total subunits are essential for electron transfer in complex III. The three essential subunits are cytochrome *b* which contains low and high potential *b*-type hemes (b_l and b_h), cytochrome c_1 which contains a *c*-type heme, and the iron –sulfur protein (ISP) which contains a 2Fe-2S (FeS) cluster.

The protonmotive Q-cycle hypothesis is commonly used to describe the way ubiquinol is used twice in proton translocation in the bc_1 complex (6, 7). Q-cycle hypothesis consists of a two substrate binding site model, a quinol oxidation (Q_o) site and a quinone reduction (Q_i) site. Bifurcation of electrons comes from a quinol at the

Q_o site where the first electron is transferred through ISP and cytochrome c_1 to the soluble electron acceptor cytochrome *c* and the second electron is transferred through hemes b_L and b_H to the Q_i site. Bifurcation of electrons is coupled to the translocation of two protons per molecule of quinol. The oxidized quinol may move to the Q_i site to become reduced. One complete Q-cycle will use two molecules of quinol and one molecule of quinone resulting in the production of one quinol molecule along with the translocation of four protons to the positive side of the membrane. Prior to the first crystal structure of the bc_1 complex, the study of various inhibitors of the bc_1 complex played an important role in elucidating the mechanics of the bc_1 complex (8, 9). The first crystal structure of cytochrome bc_1 complex from bovine heart mitochondria was solved at 2.9 Å resolution (10). Afterwards, more complete bc_1 complex structures were reported (11-13). In spite of intense efforts by many investigators none of the crystal structures of the bc_1 complex show quinol or quinone in the Q_o site as predicted by the Q-cycle. However, some of the crystal structures show various non-competitive inhibitors in the Q_o (9).

It is important to note that the protonmotive Q-cycle hypothesis was developed before the first crystal structure of the bc_1 complex was solved, which would have allowed for a more effective analysis of the geometry of the active sites. Considering the resources available at the time of the development of the proton motive Q-cycle hypothesis, it is astounding to see the predictive power of the Q-cycle hypothesis in effect now that structural data is available. The Q-cycle hypothesis adequately describes a mechanism for a two separate substrate binding site model in the bc_1 complex, and these two separate binding sites are also confirmed from the crystal

structures with inhibitors for the Q_o and Q_i sites. However, there have not been any experiments to rule out the possibility of more than two binding sites for the substrates in the bc_1 complex. A study using NMR methods recognizes that three molecules of the substrate bind to the bc_1 complex (14). Azido-Q labeling studies also reveal the existence of more than two binding sites in the bc_1 complex. Thus, in order to understand how the bc_1 complex functions correctly, it is critical to have a detailed understanding of the correct number and location of binding sites for the substrates. In order to unambiguously detect and confirm this third binding site an active quinol analog was synthesized with a bromine atom substituted in the place of the methyl group on the quinol ring. The bromine will serve as the anomalous signal tracing device to allow for the detection of the position and orientation of the active quinol analog. X-ray diffraction data was collected at a wavelength slightly above the bromine edge to allow for the detection of the bromine anomalous signal in the x-ray diffraction data. Preliminary kinetics studies show 2-Bromo-5,6-dimethoxy-3-pentyl-benzene-1,4-diol (2BrQ) initially active in the bc_1 complex and at higher concentrations 2BrQ will start inhibiting the bc_1 complex. X-ray crystallographic analysis of the bc_1 complex crystals prepared with 2BrQ show an anomalous signal for the bromine in a third substrate binding site separate from the Q_i and Q_o sites described in the Q-cycle model. This binding site is located in the same region as revealed by azido-Q labeling experiments (15). When the 2BrQ is combined with 2-(10-Bromo-decyl)-5,6-dimethoxy-3-methyl-benzene-1,4-diol (QC10Br) in bc_1 complex crystals the anomalous signal for the 2BrQ shows up in a new third binding site and the QC10Br is detectable in the Q_o site.

MATERIALS AND METHODS

Mitochondrial bc_1 complex crystal growth

Cytochrome bc_1 complex from the bovine heart mitochondria was prepared as previously reported (16,17). To remove impurities and enhance crystallization of the bc_1 complex, bc_1 particles are subjected to an additional 15-step ammonium acetate fractionation. Pure bc_1 complex is recovered from precipitates formed between 18.5% and 33.5% ammonium acetate saturation; the pure bc_1 complex is then dissolved in 50 mM Tris-HCl buffer, pH 7.8, containing 0.66 M sucrose to a protein concentration of ~30mg/ml and stored at -80^{o}C until used for crystallization. Concentrations of cyt c_1 and cyt *b* are determined spectroscopically, using millimolar extinction coefficients of 17.5 cm^{-1} mM^{-1} and 28.5 cm^{-1} mM^{-1} respectively.

For crystallization the frozen solutions of purified bc_1 complexes were allow to thaw on ice and were then adjusted to a concentration of ~ 18mg/ml in a buffer of 50 mM Mops at pH 7.2, 20 % (v/v) glycerol, 20 mM ammonium acetate, and 0.16% (w/v) sucrose monocaprate. For co-crystallization experiments 2BrQ analogues were added to bc_1 complex samples that were either partially reduced where cyt c_1 was ~18% reduced or the bc_1 complex sample was pre-oxidized with ferricynite before the addition of 2BrQ. Then the solution was allowed to sit over night at 4^{o}C and sitting drop plates from Hampton were set up using 30uL of solution in the sitting drop and 100uL of equilibrating solution in the well. The crystallization setup is also described in previous publications (10, 16). Crystals appeared in two weeks and the sizes of the crystals ranged from 0.3mm to 1.2mm. To prevent the formation of ice build-up on

the crystals when the crystals are frozen, the crystals were cryo-protected at a glycerol concentration of 33% (w/v).

X-ray diffraction data collection and reduction

Complete sets of data were obtainable at synchrotron radiation sources when cryocooled to 100K. To optimize the bromine anomalous scattering signal, data was collected at around 0.907 angstroms slightly below the bromine absorbance edge in angstroms of (0.9202 angstroms). All of the data used in this work was collected at the Advance Photon Source, Argonne National Laboratory on the 17-ID IMCA-CAT beam line. Raw diffraction data was processed with Mosflm, and integrated intensities were merged and scaled with SCALA which are part of the CCP4 package (18-20).

Data analysis and structure refinement

Structure refinement for the data was carried out with the REFMAC program (21). The starting atomic coordinates of the native bc_1 complex were used for the initial phasing of the model followed by rigid body, iterative maximum likelihood and TLS (translation, libration, and screw tensor) refinement. Between refinement sigma A weighted 2Fo-Fc, Fo-Fc, and anomalous difference maps were calculated and used in the program Xfit from the XtalView package where model corrections were made (22). Atomic models for the substrates were generated in the CCP4 sketcher module if library files did not already exist for the substrate.

RESULTS AND DISCUSSION

Conformation of an Active Q_m Binding Site

2BrQ is initially active in the bc_1 complex and at higher concentrations 2BrQ will start inhibiting the bc_1 complex. Reduced 2BrQ is still capable of passing electrons to the bc_1 complex, and at higher concentrations 2BrQ will start inhibiting the bc_1 complex. This intrinsic property of 2BrQ will allow for the ability to decipher details of the initial reduction of the bc_1 complex once the location and position of this 2BrQ is resolved in the bc_1 complex crystal structure. When the number of carbon atoms in the alkyl substituent on the 2BrQ is decreased there is an observed decrease in the enzymatic activity of the bc_1 complex. This decrease in activity proved to be a powerful property in allowing for the detection of the 2BrQ molecule in the diffraction data. Initial attempts to co-crystallize 2-Bromo-5,6-dimethoxy-3-decyl-benzene-1,4-diol ($2BrQ_{10}$) did not yield significant peaks in the anomalous difference map; however the use of 2BrQ was successful. It seems the lower activity of the 2BrQ may be related to the ability of 2BrQ to spend more time in the binding site versus the time spent in the binding site of $2BrQ_{10}$ thus allowing for its detection in the x-ray diffraction data.

2BrQ confirms existence of a third substrate binding site

To determine where the initial binding site of 2BrQ binds, oxidized crystals were soaked with 2BrQ. X-ray diffraction data was collected at a wavelength slightly above the bromine edge to allow for the definitive unambiguous detection of 2BrQ in the bc_1 complex. An anomalous difference map was calculated and a (5 sigma) anomalous peak for the bromine was detected in the Q_m binding site (Figure 1). The FeS anomalous signal was diminished significantly, which has been shown to represent the oxidized state of the enzyme (17). From the difference map (F_o-F_c) it appears that the hydroxyl group on the 2BrQ is hydrogen bonding with the (backbone carbonyl oxygen atom of residue of Ser 297) suggesting a possible mode of catalytic action in this third substrate binding site for the removal of the 2BrQ hydroxyl hydrogen atom. The 2BrQ molecule is 9.54 angstroms from the edge of heme b_H and 15.70 angstroms from the edge of heme b_L and 20.13 angstroms from the iron sulfur cluster. This data also reveals the binding of the native substrate ubiquinol in the Q_o site and ubiquinol with 2 isoprene groups in the Q_i site (Figure 2,3). The Fo-Fc difference map revealed enough map density to allow for the modeling in of all ten isoprene groups as seen in figure 2.

2BrQ + QC10Br Co-Crystallization

In order to determine whether the binding of the 2BrQ in the Q_m site might have an effect on the ability of quinol to bind in the Q_o site 2BrQ and 2-(10-Bromo-decyl)-5,6-dimethoxy-3- methyl-benzene-1,4-diol (QC10Br) was co-crystallized with the oxidized bovine bc_1 complex and x-ray diffraction data were collected slightly above the absorbance edge for the bromine atom.

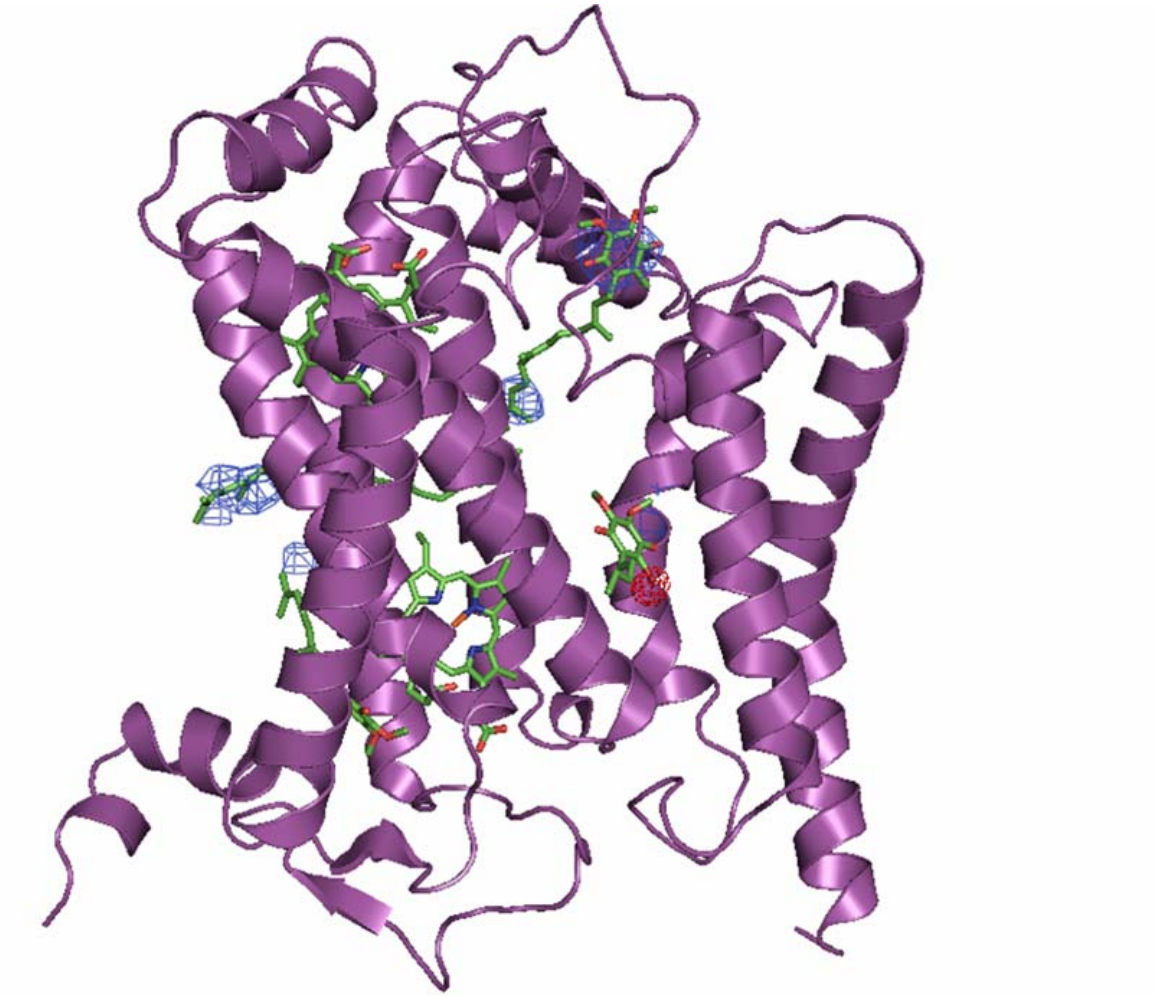

Figure 1. 2BrQ binding in the Q_m site. The anomalous difference map is in red covering the bromine atom.

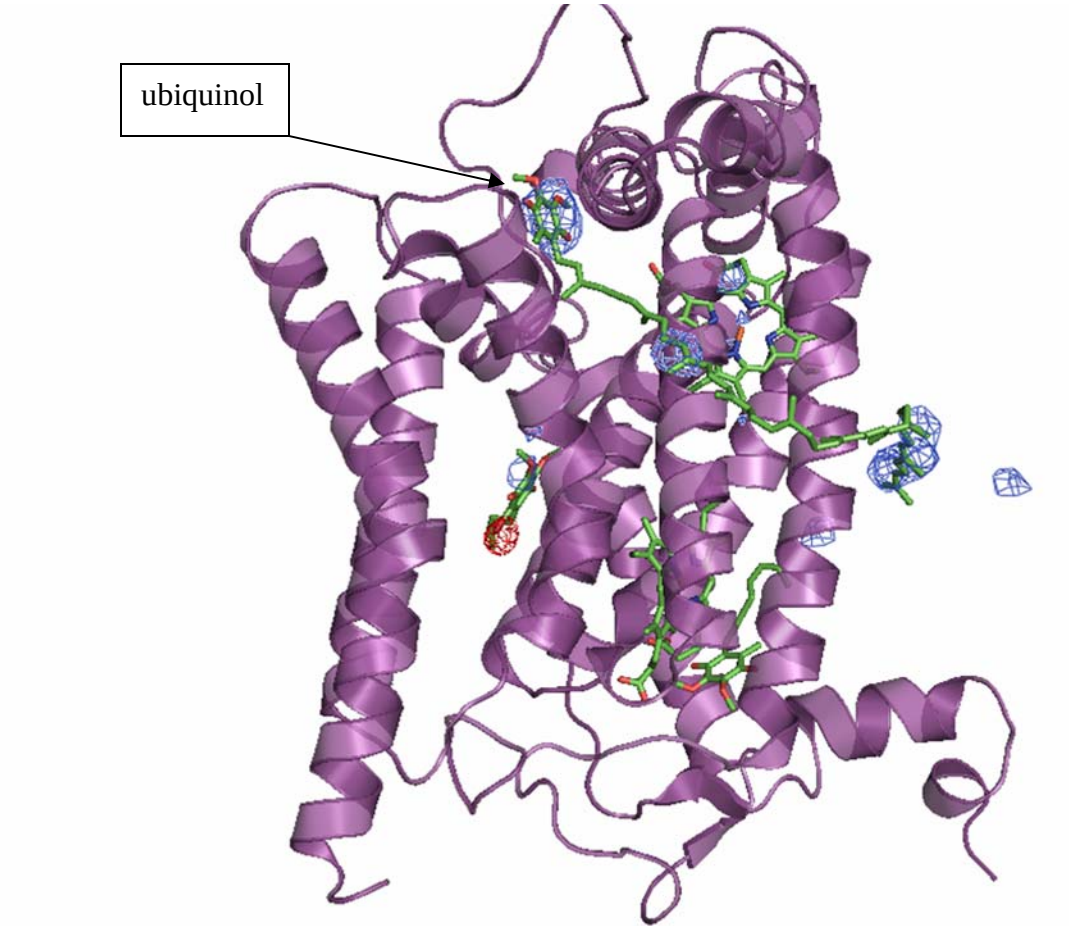

Figure 2. Q_o site native ubiquinol with ten isoprene groups modeled in. The blue density is five sigma contoured Fo-Fc density. Red density is for the anomalous signal on the 2BrQ molecule.

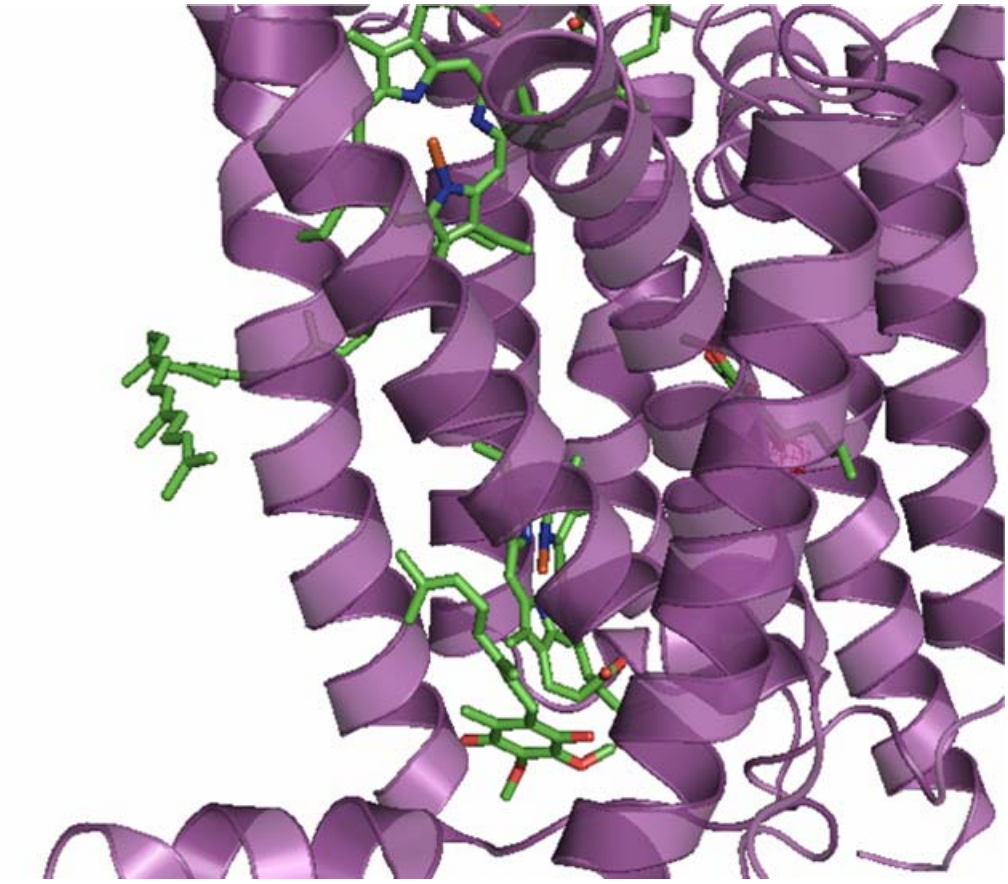

Figure 3. Q_i site quinone with two isoprene groups modeled in.

Anomalous and Fo-Fc difference maps were calculated for the 2BrQ+QC10Br data set. The anomalous map show a five sigma peak the binding of 2BrQ in the Q_m site and 4 sigma anomalous peak for the bromine on the end of the alkyl chain on QC10Br (Figure 4). In this data set the 2BrQ molecule has rotated 180 degrees, relative to the position of the 2BrQ in the other data set. This rotation is interesting in that it now places the same hydroxyl group in hydrogen bonding range of the carbonyl oxygen of residue Ser297. And the anomalous signal for the FeS is stronger indicating the bc_1 complex in a more reduced state. In figure 5, QC10Br is observed in the Q_o site with the anomalous difference map density for the bromine at the end of the ten carbon chain.

Conclusion

The combination of information gained from these two data sets allow for the explanation of a possible Q-cycle mechanism where only one ubiquinol is needed per turnover. As shown in figure 5, in step one the substrate would arrive in the Q_m binding site due to the fact that the Q_m site is the most outward facing cavity and the most easily accessible cavity of the three from the outside of the bc_1 complex figure. From the Q_m site the substrate will pass two electrons to cytochrome *b* thus reducing cytochrome *b* which is inline with the oxidant induce experiments. In the next step a oxidized ubiquinone molecule from the Q-pool will come into the Q_i site and pick up both electrons from cytochrome *b* and pick up two protons from the matrix. This step is directly inline with the oxidant induce experiments which initially show the reduction of cytochrome *b* then the oxidation of cytochrome *b*.

A

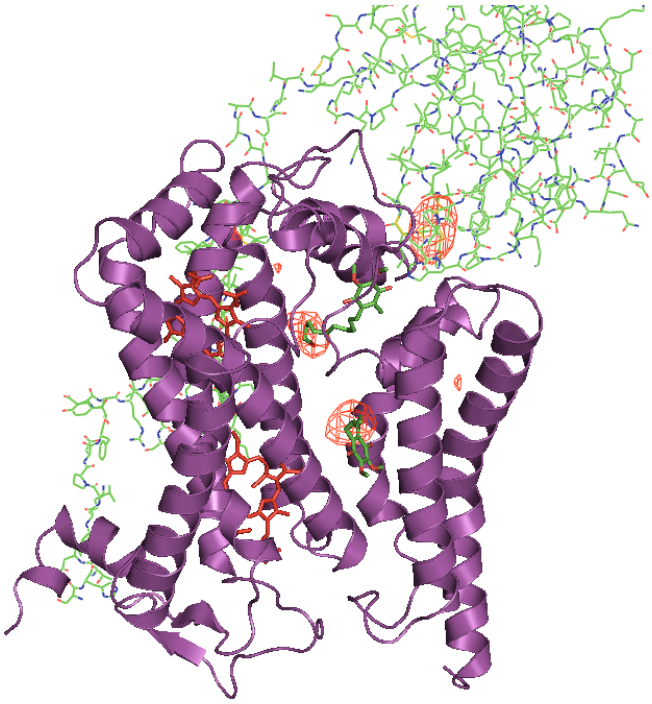

B

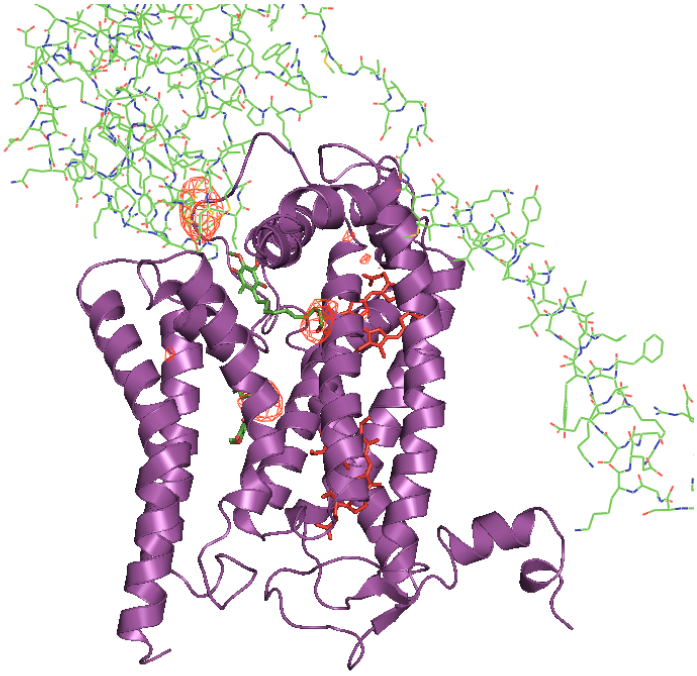

Figure 4. (A) 2BrQ binding in Q_m site with the anomalous signal for the bromine rotated 180 degrees. (B) QC10Br binding in the Q_o site. In green is the ISP subunit and the red density is from the anomalous map contoured at five sigma.

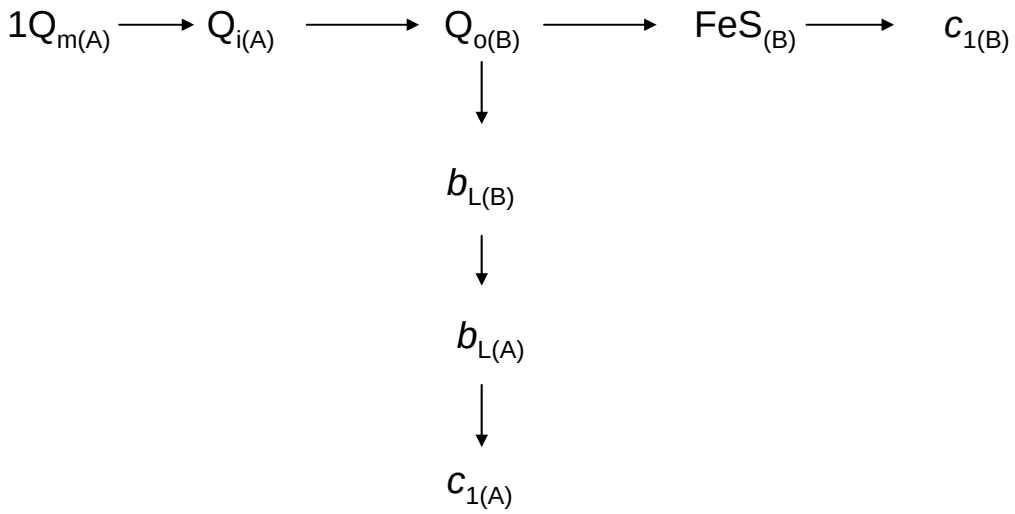

Figure 5. Schematic illustration of a possible Q-cycle mechanism. The letter (A) represents one monomer and (B) represents the other monomer in the bc_1 complex.

In the third step, the now reduced quinol in the Q_i site will now move to the Q_o site of the other monomer and now bifurcate electrons one to FeS and one to heme b_L. In the next step the electron that went to heme b_L will transfer to heme b_L on the opposing monomer and in the last step transfer the electron to heme c_1 by passing the FeS cluster to complete one turnover of the bc_1 complex from one quinol molecule.

Thus the study of this 2BrQ provides an enormous advantage over the other inhibitors used to understand how the bc_1 complex functions due to the fact that 2BrQ is initially active in the bc_1 complex and retains all the features of the quinol head group except for the methyl group substitution with bromine. Most of the inhibitors used in the development of the Q-cycle are not capable of reducing the bc_1 complex and many of the inhibitors in the Q_o site exhibit non-competitive inhibition thus making the understanding of how the actual substrate binds extremely complicated. 2BrQ offers a significant advantage, in that the identity and orientation of the compound can be easily detected in x-ray crystallographic data unambiguously by collecting anomalous data for the bromine atom. These results provide a compelling argument for the existence of a functional third substrate binding site in the cytochrome bc_1 complex. The Q_m binding site appears to be the point where the first quinol molecule comes in to reduce the bc_1 complex, thus the closest redox goup would be the cytochrome b b_H heme. And the Q_o site seems to be the where the second quinol comes in to reduce the FeS. The stoichiometry of the Q-cycle stays the same in that two quinol molecules reduce the bc_1 complex and one molecule of quinol is generated per turnover, however in this revised mechanism the quinol that is

generated is used as opposed to the quinol leaving the bc_1 complex thus requiring the bc_1 complex to wait for a second molecule of quinol to come into the Q_o site.

The fact that there is a third substrate binding site allows for an enormous advancement in the study of the how the bc_1 complex functions in the electron transfer chain. It is interesting, however, to note the original Q-cycle hypothesis does an amazing job of mapping out the functioning of the bc_1 complex under the assumption of only a two substrate binding site bc_1 complex, which the notion of only two binding sites comes mainly from the study of available inhibitors for the bc_1 complex. Of greater interest is the fact that the Q-cycle hypothesis was developed many years before the first bc_1 complex structure was solved. Further studies on the Q_m binding site are currently in progress to describe in detail the reaction mechanism taking place in the Q_m site.

REFERENCES

1. Junker, H., et al., (2005) Proteomic identification of the involvement of the mitochondrial rieske protein in epilepsy. *Epilepsia* **46**(3), 339-43.
2. Blakely, E.L., et al., (2005) A mitochondrial cytochrome b mutation causing severe respiratory chain enzyme deficiency in humans and yeast. *Febs J* **272**(14), 3583-92.
3. Fisher, N., et al., (2004) Disruption of the interaction between the Rieske iron-sulfur protein and cytochrome b in the yeast bc1 complex owing to a human disease-associated mutation within cytochrome b. *Eur J Biochem* **271**(7), 1292-8.
4. Borisov, V.B., (2004) Mutations in respiratory chain complexes and human diseases. *Ital J Biochem* **53**, 34-40.
5. Schagger, H., et al., (1986) Isolation of the eleven protein subunits of the bc1 complex from beef heart. *Methods Enzymol* **126**, 224-37.
6. Trumpower, B.L., (1990) The protonmotive Q cycle. Energy transduction by coupling of proton translocation to electron transfer by the cytochrome bc1 complex. *J Biol Chem* **265**,11409-12.
7. Mitchell, P., (1976) Possible molecular mechanisms of the protonmotive function of cytochrome systems. *J Theor Biol* **62,**327-367.

8. Link, T.A., et al., What information do inhibitors provide about the structure of the hydroquinone oxidation site of ubihydroquinone: cytochrome c oxidoreductase? *J Bioenerg Biomembr*, 1993. **25**(3): p. 221-32.
9. von Jagow, G. and T.A. Link, (1986) Use of specific inhibitors on the mitochondrial bc1 complex. *Methods Enzymol* **126**, 253-71.
10. Xia, D., et al., (1997) Crystal structure of the cytochrome bc1 complex from bovine heart mitochondria. *Science* **277**(5322), 60-6.
11. Iwata, S., et al., (1998) Complete structure of the 11-subunit bovine mitochondrial cytochrome bc1 complex. *Science*, **281**(5373), 64-71.
12. Berry, E.A., et al., (1999) Structure of the avian mitochondrial cytochrome bc1 complex. *J Bioenerg Biomembr* **31**(3), 177-90.
13. Hunte, C., et al., (2000) Structure at 2.3 A resolution of the cytochrome bc(1) complex from the yeast Saccharomyces cerevisiae co-crystallized with and anti-body Fv fragment. *Structure* **15**, 669-684.
14. Bartoschek, S., et al., (2001) Three molecules of ubiquinone bind specifically to mitochondrial cytochrome bc1 comple*x. J Biol Chem* **276**(38), 35231-4.
15. He, D.Y., L. Yu, and C.A. Yu, (1994) Ubiquinone Binding Domains in Bovine Hear Mitochondrial Cytochrome b. *J Biol Chem* **269**, 2292-2298.
16. Yu, C.A. and L. Yu, (1980) Resolution and reconstitution of succinate-cytochrome c reductase: preparations and properties of high purity succinate dehydrogenase and ubiquinol-cytochrome c reductase. *Biochim Biophys Acta*, **591**(2), 409-20.

17. Yu, C.A., et al., (2002) Inter- and intra-molecular electron transfer in the cytochrome bc(1) complex. *Biochim Biophys Acta*, **1555**(1-3), 65-70.

18. Leslie, A.G., (1992) Recent changes to the MOSFLM package for processing film and image plate data. *Jont CCP4+ESF-EAMCB Newsletter on Protein Crystallography*, No. **26**

19. Manfred W., (2001) Global indicators of X-ray data quality. *J. Appl. Cryst.* **34**, 130-135.

20. Collaborative Computational Project, Number 4. (1994) The CCP4 suite: programs for protein crystallography. *Acta Cryst*. D**50**, 760-763.

21. Murshudov, G., et al, (1997) Refinement of macromolecular structures by the maximum likelihood method. *Acta Cryst*. D**53**, 240-255.

22. McRee, D. E., (1999) XtalView/Xfit--A versatile program for manipulating atomic coordinates and electron density. *J Struct Biol* **125**, 156-165.

VITA

Byron Norton Quinn

Candidate for the Degree of

Doctor of Philosophy

Thesis: X-RAY CRYSTALLOGRAPHIC STUDIES OF THE CYTOCHROME bc_1 COMPLEX

Major Field: Biochemistry and Molecular Biology

Biographical:

Education: Graduated form Jennings Senior High, St.Louis, MO. In June 1992; Received Bachelor of Science in Chemistry from Langston University, Langston, Oklahoma; Received Master of Science in Biochemistry from Oklahoma State University, Stillwater, OK.

Experience: Employed by Oklahoma State University, Department of Biochemistry as a graduate research assistant.

Name: Byron Norton Quinn Date of Degree: December, 2006

Institution: Oklahoma State University Location: Stillwater, Oklahoma

Title of Study: XRAY CRYSTALLOGRAPHIC STUDIES OF THE CYTOCHROME bc_1 COMPLEX

Pages in Study: 88 Candidate for the Degree of Doctor of Philosophy

Major Field: Biochemistry and Molecular Biology

Scope and Method of Study: The purpose of this study was to enhance the understanding of the bc_1 complex. The method used in this study is x-ray crystallography and protein crystallization.

Findings and Conclusion: The bc_1 complex is an integral component of the electron transfer chain responsible for aiding in the production of a proton gradient for ATP synthesis. Mutations in the bc_1 complex are associated with epilepsy and other human diseases. Functioning of the bc_1 complex is commonly explained by the proton motive Q cycle. The proton motive Q cycle hypothesis makes use of only two completely separate substrate binding sites in the bc_1 complex. Crystallographic anomalous signal tracking allowed for the deciphering of a hidden third substrate binding site which may have possible implications on the electron transferring pathway in the bc_1 complex. A modified Q-cycle mechanism is proposed that makes use of the third substrate binding site.

ADVISER'S APPROVAL: Chang-An Yu